Soil moisture ~~retrieval~~ estimates at 1-km resolution making a synergistic use of ~~Sentinel-1/2/3~~ Sentinel data

Remi Madelon[1], Nemesio J. Rodríguez-Fernández[1], Hassan Bazzi[2], Nicolas Baghdadi[2], Clement Albergel[3], Wouter Dorigo[4], and Mehrez Zribi[1]

[1]CESBIO (Université de Toulouse, CNES, CNRS, IRD, INRAE), 18 av. Edouard Belin, bpi 2801, 31401 Toulouse, France
[2]TETIS, INRAE, Université de Montpellier, 34090 Montpellier, France
[3]European Space Agency Climate Office, ECSAT, Harwell Campus, Oxfordshire, Didcot OX11 0FD, United Kingdom
[4]TU Wien, Vienna, Austria

Correspondence: Nemesio J. Rodríguez-Fernández (nemesio.rodriguez@cesbio.cnes.fr)

Abstract.

~~High-resolution (HR~~ Very high-resolution ($\sim 10-100$ m) surface soil moisture (SM) observations are important for applications in ~~hydrology and~~ agriculture, among other purposes. ~~For instance, the~~ This is the original goal of the the S^2MP (Sentinel-1/Sentinel-2 derived Soil Moisture Product) algorithm, which was designed to retrieve surface SM at agricultural plot scale using simultaneously Sentinel-1 (S1) backscatter coefficients and Sentinel-2 (S2) NDVI (Normalized Difference Vegetation Index) as inputs to a neural network trained with Water Cloud Model simulations. However, for many applications, including ~~future~~ hydrology and climate impact assessment at regional level, ~~a resolution of~~ large maps with a high-resolution (HR) of around 1 km ~~is~~ are already a significant improvement with respect to most of the publicly available SM ~~data sets~~datasets, which have resolutions of about 25 km. ~~Therefore, in~~

In this study, the S^2MP algorithm was adapted to work at ~~a resolution of 1 km~~ 1-km resolution and extended from croplands ~~(cereals and grasslands)~~ to herbaceous vegetation types. A target resolution of 1 km also allows to ~~explore the use of~~ evaluate the interest of using NDVI derived from Sentinel-3 (S3) instead of S2. ~~The algorithm improvements are evaluated both over Europe and other regions of the globe, for which S1 coverage is poorer.~~

Two sets of SM maps at 1-km resolution were produced with S^2MP over ~~six~~ 6 regions of $\sim 10^4$ km^2 in the southwest and southeast of France, Spain, Tunisia, North America, ~~as well as Australia from 2017 to~~ and Australia for the whole year of 2019. The first set ~~of maps~~ was derived from the combination of S1 and S2 data (S1+S2 maps), while the second one was derived from the combination of S1 and S3 (S1+S3 maps). S1+S2 and S1+S3 SM maps were compared to each other~~and~~ , to those of the 1-km resolution Copernicus Global Land Service (CGLS) SM and Soil Water Index (SWI) ~~data sets as well as to~~ datasets, and to those of the SMAP+S1 product.

The S^2MP S1+S2 and S1+S3 SM maps are in very good agreement in terms of correlation ($R \geq 0.9$), bias (≤ 0.04 m^3 m^{-3}) and standard deviation of the difference ($STDD \leq 0.03$ m^3 m^{-3}) over the 6 domains investigated in this study. ~~The~~ In a second step, the S1+S3 S^2MP maps were compared to the other HR maps. S1+S3 SM maps are well correlated to ~~those from~~ the CGLS SM ~~product~~ maps ($R \sim 0.7$-0.8), but the correlations with respect to the other HR maps (CGLS SWI and SMAP+S1) drop significantly over many areas of the 6 domains investigated in this study. ~~In addition, higher~~ The highest correlations

between the HR maps were found over croplands and when the 1-km pixels have a very homogeneous land cover. The bias in between the different maps was found to be significant over some areas of the six domains, reaching values of $\pm$ 0.1 $m^3\ m^{-3}$. The S1+~~S2~~ S3 maps show a lower STDD with respect to CGLS maps ($\leq$ 0.06 $m^3\ m^{-3}$) than with respect to the SMAP+S1 maps ($\leq$ 0.1 $m^3\ m^{-3}$) for all the 6 domains.

Finally, all the HR ~~data sets~~ datasets (S1+S2, S1+S3, CGLS and SMAP+S1) were also compared to ~~in situ~~ in-situ measurements from 5 networks across 5 countries along with coarse resolution (CR) SM products from SMAP, SMOS and the ESA Climate Change Initiative (CCI). While all the CR and HR products show different bias and STDD, the HR products show lower correlations than the CR ones with respect to ~~in situ measurements.~~

in-situ measurements. The discrepancies in between the different HR datasets except for the more simple land cover conditions (homogeneous pixels with croplands) and the lower performances with respect to in-situ measurement than coarse resolution datasets, show the remaining challenges for large scale HR SM mapping.

1 Introduction

Surface soil moisture (SM) plays a key role in the Earth water cycle as it affects many hydrological processes such as infiltration, runoff, evaporation and precipitation (Koster et al., 2004). SM ~~is~~ measurements are used to constrain numerical weather prediction (NWP) models via data assimilation (De Rosnay et al., 2013; de Rosnay et al., 2014; Rodríguez-Fernández et al., 2019) ~~. It is also used~~ as well as for crop yields forecasting, food security and agriculture management (Guerif and Duke, 2000). SM was identified as one of the 50 "essential climate variables" (ECVs) by the Global Climate Observing System in the context of the United Nations Framework Convention on Climate Change (Plummer et al., 2017; GCOS, 2021). Building long time series of SM is crucial for climate applications, and this is the goal of projects such as the European Space Agency's Climate Change Initiative (ESA CCI) for SM (Gruber et al., 2019).

Both active and passive microwave sensors can be used to estimate SM at coarse resolutions ($\sim$ 25-40 km) including the active Advanced Scatterometer (ASCAT, Vreugdenhil et al., 2016), the passive Advanced Microwave Scanning Radiometer 2 (AMSR2, Kim et al., 2015; Imaoka et al., 2000) and the two sensors that have ~~specifically been~~ been specifically designed to measure SM at L-band: the Soil Moisture and Ocean Salinity (SMOS, Kerr et al., 2012) and Soil Moisture Active Passive (SMAP, Entekhabi et al., 2010). However, despite the actual availability of these SM products, they do not match the requirements of a number of applications. Peng et al. (2020) have discussed a road-map and requirements for future SM products. An optimal spatial resolution for data assimilation into NWP models and reanalysis would be 5-10 km (global models are already running with resolutions better than 10 km, see for instance Muñoz-Sabater et al., 2021). The evaluation of climate models and the assessment of climate change impacts at regional level would also benefit from a higher resolution than that of the current generation of coarse resolution sensors. In addition, other applications in hydrology, agriculture and risk assessment require even higher resolutions of $\sim$ 1 km (Massari et al., 2021).

Downscaling the coarse scale resolution data by merging them with higher resolution data is a possibility to achieve high ~~resolutions SM data sets~~resolution SM datasets. For example, ~~it can be done using~~ high resolution SM estimates can be derived

from visible/infrared ~~data (Merlin et al., 2012) or using~~ (Merlin et al., 2012) or Synthetic Aperture Radar (SAR, Tomer et al., 2016; Das et al., 2019) measurements. SAR observations alone have also been tested to estimate SM using different frequencies and instruments such as RadarSAT, ALOS-L or TerraSAR-X. Radar signal is sensitive to the dielectric constant linked to SM but also to surface geometry (including roughness) and vegetation water content and structure (Ulaby et al., 1986). Different inversion algorithms have been proposed considering principally three techniques: change detection algorithms (Wagner et al., 1999; Balenzano et al., 2010; Bauer-Marschallinger et al., 2018), direct inversion of physical or empirical models (Moran et al., 2000; Srivastava et al., 2009; Pierdicca et al., 2010; Hajj et al., 2014; Bousbih et al., 2017; Şekertekin et al., 2018) and finally machine learning methods ~~(El Hajj et al., 2017)~~(Paloscia et al., 2004; Notarnicola et al., 2008; El Hajj et al., 2017).

With the successive launches of the C-band SARs onboard Sentinel-1 A (~~S1-A~~S1A, 2014) and Sentinel-1 B (~~S1-B~~S1B, 2016), SM can be estimated at high spatial resolution and with a revisit time better than 6 days over Europe. Three operational high resolution (HR) SM ~~data sets~~ datasets at 1-km resolution using S1 exist such as the S1 ~~1-km~~ SM and Soil Water Index (SWI) products from the Copernicus Global Land Service (CGLS, Bauer-Marschallinger et al., 2018, 2019) and the SMAP+S1 downscaled product (Das et al., 2020)~~with resolutions of 1 or 3 km~~. SM estimates at a very high resolution (~~plot~~ 10-m scale) at some locations in Europe (as well as in Lebannon and Morocco) over croplands are also distributed by the French continental surfaces data center (THEIA, https://www.theia-land.fr). In contrast to the CGLS ~~data set~~datasets, the THEIA SM ~~data set is obtained making a synergistic use of~~ dataset is obtained using synergistically S1 and Sentinel-2 (S2) ~~using the~~ measurements as inputs to the Sentinel-1/Sentinel-2 derived Soil Moisture Product (S^2MP) algorithm (El Hajj et al., 2017). This ~~data set~~ dataset has been evaluated against ~~in situ data in~~ in-situ measurements in comparison to SMAP, SMOS and ASCAT coarse resolution ~~data sets~~ (CR) datasets (El Hajj et al., 2018) and with respect to the CGLS S1 SM ~~data set~~ dataset (Bazzi et al., 2019), both in the south of France. The S^2MP SM estimates showed the lowest unbiased root mean squared errors with respect to ~~in situ~~ in-situ measurements but also a moderate correlation, lower than that obtained for SMAP and ASCAT ~~data sets~~ datasets (El Hajj et al., 2018). In this region, the S^2MP SM showed better performances with respect to ~~in situ~~ in-situ measurements than the CGLS SM for the classical metrics (Bazzi et al., 2019).

Taking into account the importance of having accurate HR ~~SM data sets, a more comprehensive evaluation of existing products must be done over different types of surfaces and regions. It is worth noting that even if the current temporal coverage of the S1 data is relatively short, it is also essential to evaluate their potential future use for climatic applications. For this and other applications mentioned above a resolution of~~ large scale SM datasets, in this study the S^2MP algorithm was extended to provide SM estimates over both croplands and herbaceous vegetation at 1-km ~~is a breakthrough with respect to existing data sets. Moreover, this target resolutionalso makes possible~~ resolution, which also allowed to use Sentinel-3 (S3) NDVI ~~as input to the S^2MP algorithm in addition to S1 data~~instead of S2.

~~The S1 spatial coverage and revisit time are optimized over Europe and the CGLS products only provided over Europe and Mediterranean region. However, it is interesting to evaluate the potential of Sentinel based products over other regions of the globe. Hence,~~ Two sets of SM maps at 1-km resolution were produced with the S^2MP algorithm over six domains of $\sim 10^4$ km^2 ~~were studied~~ in the southwest and southeast of France, Tunisia, North America, Spain and Australia ~~.~~ (see panel A from Figure 1). A set is based on the combination of S1 and S2 measurements (S1+S2 maps), while the other is based on

the combination of S1 and S3 measurements (S1+S3 maps). The S^2MP S1+S2 and S1+S3 maps were compared to those ~~of~~ provided by the SMAP+S1 product as well as those ~~of~~ from the CGLS SM and SWI ~~data sets.~~ datasets from January to December 2019. The comparison was carried out ~~over the 6 study regions~~ on a per pixel basis and the results were analysed according to pixel homogeneity for areas covered by croplands and herbaceous vegetation. In addition, the HR time series were evaluated against ~~in situ data~~ in-situ measurements along with those of coarser resolution SM ~~data sets~~ datasets from SMAP, SMOS, and ESA CCI.

The paper is structured as follows. Section 2 presents the different remotely sensed and ground based data that are used in this study. Section 3 describes the methodology used to estimate SM over croplands and herbaceous regions using S1+S3. Section 4 shows the ~~results of the comparisons of the HR~~ S1+S3 S^2MP maps and time series. They are also compared to the S1+S2 maps as well ~~the assessment against in situ~~ as to other HR datasets, coarse resolution datasets and in-situ measurements. Section 5 discusses the interest of the S^2MP algorithm modifications and the remaining challenges for large scale HR SM mapping. Section 6 draws the conclusions of the study.

2 Data

2.1 ~~High resolution soil~~ Soil moisture ~~products~~maps computation

2.1.1 ~~S^2MP~~

~~The S^2MP (~~

2.1.1 Sentinel-1

The Sentinel-1 ~~/Sentinel-2 derived Soil Moisture Product) algorithm (El Hajj et al., 2017) estimates surface SM at the scale to agricultural plots using synergistically radar signal and optical images from S1~~ mission is the first satellites constellation mission of the Copernicus program and was conducted by ESA. The mission is composed of a constellation of two satellites sharing the same orbital plane. S1A was launched on 3 April 2014, and S1B on 25 April 2016. They were placed in a near-polar, sun-synchronous orbit. The revisit frequency is 12 days over Europe (6 days using both satellites) with crossing time at equator at 6:00 pm for the descending overpass. S1A and ~~S2 satellites as inputs to a neural network. The neural network is trained using a synthetic database gathering *(i)* SAR~~ S1B carry onboard a C-band ~~backscatter coefficients in the VV polarization *(ii)* incidence angles (from 20 to 45 degrees), and *(iii)* NDVI (Normalized Difference Vegetation Index) as input and SM examples as target. This synthetic database is built using a Water Cloud Model (Baghdadi et al., 2017) combined with an Integral Equation Model (Baghdadi et al., 2006, 2011) that are specially modified and optimized for this application.~~ (wavelength 6 cm) SAR imaging instrument, enable to acquire imagery regardless of the weather and the time of the day.

~~In the framework of this study, the trained neural networks were applied to a real database gathering SAR~~ For the production of the S^2MP SM maps, S1A and ~~NDVI measurements computed from S1 and S2 over croplands and herbaceous vegetation areas at 100-m resolution using the CGLS land cover map. It does not consider retrievals for other types of land cover.~~

Afterwards, the data were averaged at 1-km resolution to provide HR SM maps(hereafter S^2MP_{S1S2}) over the six $\sim 10^4$ km^2 regions of the study. The S^2MP algorithm was also adapted to work directly at 1-km resolutionusing NDVI from S3 instead of S2 to produce maps for the same six regions (hereafter S^2MP_{S1S3}, see Sect. 3.1) S1B SAR images were collected over each region of study. S1 images are accessible from the Copernicus Open Access Hub. The S1 images (10 m x 10 m) were acquired in the Interferometric Wide-swath (IW) imagining mode with VV and VH polarizations and the S1 Toolbox (S1TBX) developed by ESA was used to calibrate the images. This calibration aims to convert digital number values from S1 images into backscattering coefficients ($\sigma°$) in a linear unit and ortho-rectifying the images using the Shuttle Radar Topography Mission (SRTM) Digital Elevation Model (DEM) at 30-m spatial resolution. A database of S1 images available from January to December 2019 was created for each region of study. The databases contain S1 images acquired both in ascending (afternoon) and descending (morning) modes.

2.1.2 SMAP/Sentinel-1 L2Sentinel-2

Soil Moisture Active Passive (SMAP) was launched on 31 January The Sentinel-2 A and B (S2A and S2B) satellites were launched on 23 June 2015 by NASA (National Aeronautics and Space Administration). It carries on board a passive radiometer operating at 1.4 GHz (L-band), and a synthetic-aperture radar (active instrument) operating at 1.2 GHz. The respective spatial resolutions of the two instruments are 40 km and 1 to 3 km, however the radar stopped working a few months after launch. SMAP provides passive measurements of the land surface SM in vertical and horizontal polarizations at a fixed incidence angle of 40 degrees (Entekhabi et al., 2014).SMAP ascending and descending orbits cross the equator at 6and 7 March 2017, and were placed in a near-polar, sun-synchronous orbit. The revisit frequency is 10 days (5 days with 2 satellites) and the descending orbit crossing time at equator is at 10:00 pm and 30 am. The spatial coverage ranges from 56° S to 84° N. The satellites carry onboard a multi-spectral instrument with 13 bands: 4 bands at 10-m, 6 :00 am respectively, and the maximum revisit period is bands at 20-m and 3 days. bands at 60-m spatial resolution. The orbital swath width is 290 km (Spoto et al., 2012).

The SMAP+For the production of the S^2MP SM maps based on S1 and S2, optical images from S2A on dates close to S1 L2 V001 product (hereafter $SMAPS1$)provides SM at 1-km and 3-km resolution that are estimated using the SMAP Enhanced L3 V004 Half-Orbit at 9-km resolutionSAR images (less than 2 weeks) were downloaded from the French land data service center (Theia) website (https://www.theia-land.fr/). The S2A optical images (10 m x 10 m) are corrected for atmospheric effects and ortho-rectified.

2.1.3 Sentinel-3

The Sentinel-3 A and B (S3A and Copernicus S1A and S1B C-band SAR data (Das et al., 2020). Brightness temperatures from SMAP are disaggregated on the 1-km and 3-km EASE-Grid by using the S1 radar backscatter data and HR SM retrievals are obtained using the SMAP Active-Passive algorithm. Data are split in two different sets. The first set only uses the closest data in time from SMAP descending orbits to spatially match up with the S1 scene. While the second set uses the closest data in time between descending (6S3B) satellites were launched on 16 February 2016 and on 25 April 2018, respectively. The S3 satellites orbit is a near-polar, sun-synchronous orbit with crossing time at equator at 10:00 am) and ascending (6:00 pm)

orbits. The second data set at am for the descending overpass. They carry onboard an optical instrument payload, the Ocean and Land Colour Instrument (OLCI), that samples 21 spectral bands ([0.4-1.02] μm) with a swath width of 1 270 km and a spatial resolution of 300 m. They also carry a dual-view scanning temperature radiometer at 500-m spatial resolution: the Sea and Land Surface Temperature Radiometer (SLSTR). The revisit frequency of these instruments is 2 days when both satellites are used together (Donlon et al., 2012).

In this study, the S3 10-days synthesis NDVI at 1-km resolution was considered in this study. spatial resolution were used for the production of the S^2MP SM maps based on S1 and S3. These data are accessible in the SY_2_V10 product (Henocq et al., 2018) and were downloaded from the Copernicus Open Access Hub. The data from this product rely upon the synergistic use of the OLCI and SLSTR instruments. The product provides a 1-km VEGETATION-like product including 10-day synthesis surface reflectances and NDVI. The NDVI values correspond to a maximum NDVI value composite of all segments received for 10 days.

2.1.4 Copernicus Global Land Service products

2.2 Data used for evaluation

The Copernicus Global Land Service

2.2.1 Copernicus Global Land service

Two CGLS datasets were used to compare with the S^2MP maps:

(*i*) The CGLS V111 S1 Surface Soil Moisture product (hereafter $CoperSSM$) is retrieved from the S1 radar backscatter images estimations over the European continent at 1-km resolution (Bauer-Marschallinger et al., 2019). The images are acquired at C-band SAR in VV polarization, and the retrieval approach is based on a change detection algorithm (Bauer-Marschallinger et al., 2018). Changes observed in the C-band SAR backscatter coefficient are interpreted as changes in the SM values, whereas other surface properties such as the geometry, surface roughness and vegetation cover are interpreted as assumed to be static in time for each pixel. The algorithm provides local relative SM values in percentages ranging between 0% and 100% except in the case of extremely dry conditions, frozen soil, snow-covered soil and flooding. The data are sampled at 1-km resolution from 11°W to 50°E and from 35°N to 72°N.

The Copernicus Global Land Service (*ii*) The CGLS V101 S1 Soil Water Index product (hereafter $CoperSWI$) is derived from a fusion of surface SM observations from S1 C-band SAR and Metop ASCAT sensors (Bauer-Marschallinger et al., 2018). It uses a two-layer water balance model that is adapted to use a recursive formulation and does not account for soil texture. A Surface State Flag (SSF) that indicates frozen/unfrozen/melting state of the surface, depending on the temperature, is used to identify SM values under non-frozen conditions to be used for the SWI calculation. SWI and quality flag values are calculated based on a phenomenological formulation that depends on a parameter the characteristic time length parameter (hereafter T. An increased). A large T value is either due to represents an increase in reservoir depth or a decreased pseudo-diffusivity coefficient. This means that, for a fixed pseudo-diffusivity constant, an increased T value represents a deeper soil layer (Paulik

et al., 2014). SWI estimations for eight different T values are provided within the product. Previous evaluations of SWI data by Paulik et al. (2014) and Albergel et al. (2008) showed that the best agreement with ~~in situ~~ in-situ measured surface SM is usually obtained with T values in the range of 5-10, therefore SWI data with $T = 5$ were used in this study.

2.3 ~~Coarse resolution soil moisture products~~

2.2.1 SMAP products

~~In addition to the $SMAPS1$ product (see Sect **??**), several coarse resolution data sets~~ SMAP provides passive measurements of 1.4 GHz brightness temperatures in vertical and horizontal polarizations at a fixed incidence angle of 40 degrees with a resolution of $\sim$ 45 km (Entekhabi et al., 2014) SMAP ascending and descending orbits cross the equator at 6:00 pm and 6:00 am respectively, and the maximum revisit period is 3 days. Several HR and CR SM datasets from SMAP were used for ~~comparison purposes~~the evaluation of the S^2MP maps:

(*i*) ~~the~~ The SMAP L3 V6 SM product (hereafter $SMAPL3$). It is a daily gridded composite of the SMAP L2 V5 SM files (O'Neill et al., 2018, 2019b). Only SM ~~retrievals~~ estimates derived from L1C brightness temperatures (Chan et al., 2018) using the Single Channel Algorithms V-polarization (Entekhabi et al., 2010) were considered. SMAP L3 data are sampled at 36-km resolution.

(*ii*) ~~the~~ The SMAP Enhanced L3 V1 SM product (hereafter $SMAPL3E$), which is obtained by oversampling the L1C brightness temperatures from 36-km to 9-km resolution using ~~the Backus-Gilbert interpolation algorithm~~ an interpolation algorithm (O'Neill et al., 2019a). Only SM ~~retrievals~~ estimates derived using the Single Channel Algorithms V-polarization were considered.

2.2.2 ~~SMOS products~~

(*iii*) The SMAP+S1 L2 V1 SM product (hereafter $SMAPS1$) provides SM at 1-km resolution that are estimated using the SMAP Enhanced L3 V004 Half-Orbit at 9-km resolution and Copernicus S1A and S1B C-band SAR data (Das et al., 2020) . Brightness temperatures from SMAP are disaggregated on the 1-km EASE-Grid by using the S1 radar backscatter data and HR SM estimates are obtained using the SMAP Active-Passive algorithm. The closest data in time between descending and ascending orbits from SMAP are used to spatially match up with the S1 scene.

~~The Soil Moisture and Ocean Salinity (SMOS) mission is part of the Earth Explorer program from ESA (European Space Agency) , with contributions from CNES (Centre National d'Etudes Spatiales, France) and CDTI (Centro Para el Desarrollo Tecnológico Industrial, Spain). The satellite was launched on 2 November 2009 to measure globally and frequently the surface SM over land and sea surface salinity over the oceans (Kerr et al., 2001), with a maximum revisit time of 3 days and Equator crossings at 6:00 am and 6:00 pm for ascending and descending overpasses, respectively.~~

2.2.2 SMOS

The SMOS mission ~~relies on a two dimensional interferometric instrument~~ (Kerr et al., 2010) carries a passive interferometric radiometer operating at L-band (21 cm, 1.4 GHz) ~~able to measure brightness temperatures in both vertical and horizontal polarizations, at incidence angles from 0 to 60 degrees and~~ with a spatial resolution of 25-50 depending on the position on the field of view (43 km on average). The following ~~SMOS SM data sets~~ CR SM datasets from SMOS were used in this study:

(*i*) The CATDS SMOS L3 ~~V3~~ V7 SM product (hereafter $SMOSL3$), which is a multi-orbit SM product provided by the Centre Aval de Traitement des Données (CATDS) with a grid resolution of 25 km (Al Bitar et al., 2017). The SM retrieval process is based on the algorithm used for the SMOS L2 product (Kerr et al., 2012) ~~, and focuses on the iterative minimization of the difference between a forward model and the brightness temperatures. The model uses the $\tau - \omega$ (optical depth-single scattering albedo) approach to take into account the effect of vegetation. In contrast to the L2 algorithm, the L3 one uses~~ but using simultaneously three orbits within a one week period to better constrain the SM and ~~VOD (vegetation optical depth) estimations. The data are sampled at 25-km resolution.~~ optical depth estimations.

(*ii*) The ESA SMOS Near Neal Time (NRT) Neural Network (NN) V2 SM product (hereafter $SMOSNRT$), provided on the icosahedral equal area grid (ISEA4H9) with 15-km resolution (Rodríguez-Fernández et al., 2017). It is designed to provide SM in less than 3.5 h after sensing. The algorithm uses a ~~neural network (NN)~~ NN trained using SMOS L2 SM data (Kerr et al., 2012). The input data for the NN are SMOS brightness temperatures with incidence angles from 30 to 45 degrees for horizontal and vertical polarizations and soil temperature in the 0–7 cm layer from the European Centre for Medium-Range Weather Forecasts (ECMWF) models.

2.2.3 ESA CCI COMBINED product

In the COMBINED product of ESA SM CCI ~~version 5.2 (hereafter $CCISM$)~~ V5.2 ~~(Dorigo et al., 2017; Gruber et al., 2019)~~ (hereafter $CCISM$, Dorigo et al., 2017; Gruber et al., 2019) L2 ~~data sets~~ datasets from different active and passive sensors are directly scaled by matching their Cumulative Density Functions (CDF) to that of the ~~GLDAS (Global Land Data Assimilation System, Rod~~ Global Land Data Assimilation System (GLDAS, Rodell et al., 2004) Noah land surface model in order to remove relative biases and harmonize their dynamical ranges. In the period of this study, ESA CCI Combined uses the H SAF active sensor products from ~~ASCAT-A and -B (Advanced Scatterometer, Wagner et al., 2013)~~ the Advanced Scatterometer A and B (ASCAT, Wagner et al., 2013) and the passive ~~sensors AMSR2 (Advanced Microwave Scanning Radiometer 2, Kim et al., 2015; Imaoka e~~ ~~, SMAP,~~ sensor products from the Advanced Microwave Scanning Radiometer 2 (AMSR2, Kim et al., 2015; Imaoka et al., 2000) , as well as those from SMAP and SMOS. SM data from the passive sensors are estimated using the Land Parameter Retrieval Model (LPRM) ~~version 6~~ V6 (Van der Schalie et al., 2016, 2017). The data are sampled at 25-km resolution.

2.3 ~~Land cover map~~

~~The~~

2.2.1 Land cover

The Copernicus Global Land Service (CGLS) V3 Dynamic Land Cover Map product ~~version 3 provided by CGLS was used to evaluate the different HR and CR data sets. As described above, it is the same land cover map used by the S^2MP algorithm for this study. This product~~ delivers a global land cover map at 100-m resolution covering the period between 2015 to 2019 (Buchhorn et al., 2020). For each year, a land cover map is provided with three different levels of classes: 11 classes at level 1 (all types of forests are considered as an unique land cover class), 13 classes at level 2 (forests are splitted in two land cover classes: open and closed forests) and up to 22 classes at level 3 (all types of open and closed forests are considered). In this study, only the 2019 land cover map at level 1 was considered. The panel B of Figure 1 shows the 7 land cover classes that are represented in the ~~six~~ 6 regions of study. In this figure, the land cover map was aggregated from 100-m to 1-km resolution for evaluation purposes meaning that only the dominant land cover for each 1-km^2 pixel is shown.

2.3 ~~in situ data~~

2.2.1 In-situ measurements

The evaluation against ~~in situ measurements~~ in-situ measurements of soil moisture was performed using data from the REMEDHUS (Gonzalez-Zamora et al., 2018), SMOSMANIA (Calvet et al., 2007), OZNET (Smith et al., 2012; Young et al., 2008), USCRN (Bell et al., 2013), ARM (Cook, 2016, 2018) and the Merguellil networks ~~(Gorrab et al., 2015)~~ (**?**Gorrab et al., 2015) that are located within the six regions of this study (Table 1). All the data, except those from the Merguellil network, were retrieved from the International Soil Moisture Network (ISMN, Dorigo et al., 2011, 2021). Only sensors between 0 and 5 cm depth were considered. In total, ~~43 ISMN and 6~~ 65 ISMN and 5 Merguellil sites were used for the ~~evaluation (Table 1).~~ scaling of the $CoperSSM$ and $CoperSWI$ data (Sect. 3.2). Less sites (40 from ISMN and 2 from Merguellil) were used to assess the remotely sensed data following the criteria explained in Section 3.3. The different in-situ stations can be located using the panels A and B from Figure 1.

3 Methods

3.1 Building S^2MP maps using NDVI derived from ~~Sentinel-2 and~~ Sentinel-3

The ~~S^2MP algorithm for soil moisture estimation requires as input values the~~ S^2MP algorithm (El Hajj et al., 2017) was originally designed to estimate surface SM at the scale of agricultural plots (10-m resolution) using synergistically data derived from S1 radar signal and S2 optical images as inputs to a neural network. The neural network was first trained using a synthetic database gathering *(i)* SAR C-band backscatter coefficients in the VV polarization *(ii)* incidence angles (from 20 to 45 degrees), and *(iii)* NDVI as inputs and SM examples as target. This synthetic database was built using a Water Cloud Model (Baghdadi et al., 2017) combined with an Integral Equation Model (Baghdadi et al., 2006, 2011) that was specially modified and optimized for this application. Then, the S^2MP algorithm was applied to a real database gathering the SAR backscatter

coefficient in VV polarization from S1, the incidence angle of the SAR ~~acquisition~~ acquisitions and the NDVI derived from optical images ~~. The NDVI could be either derived from~~ taken by S2 ~~or S3 images. In this study, the use of the S2 and S3 NDVI was tested for soil moisture estimation using the S^2MP. In the first version of the S^2MP algorithm, NDVI values required as input for the neural network are derived from S2 optical images. The NDVI was first calculated~~ as follows. Firstly, the NDVI was computed at 10-m spatial resolution (native resolution of ~~the~~ S2) using the atmospherically and ortho-rectified S2 images. To overcome the cloud cover issue present in optical images, a gap filling was performed using the linear interpolation to obtain two cloud-free NDVI images per month (1st and 15th of each month). ~~Over each study site and at each~~ To derive S2 NDVI data at the S1 acquisition ~~, the~~ dates, a linear interpolation was performed for each S2 pixel using the NDVI values corresponding to the closest S2 images acquired before and after the S1 date. Secondly, the 10-m resolution S1 backscattering signal, incidence angle and S2 NDVI ~~(nearest NDVI date to the S1 date) are~~ were averaged for each 100-m ~~masked land cover pixels (cropland and herbaceous vegetation). The~~ pixels from the CGLS land cover map. Then, the SM estimation using the S^2MP algorithm ~~is thus obtained~~ was performed at 100-m spatial resolution ~~. The~~ over pixels covered by croplands using the CGLS land cover map described above (see Sect. 2.2.1). There is no retrieval for other types of land cover.

In contrast to the (El Hajj et al., 2017) approach described above, in the current study S1+S2 maps were also computed for 100-m pixels covered by herbaceous vegetation. In addition, the 100-m SM estimations were ~~then aggregated~~ aggregated to 1-km. On the other hand, HR SM maps were also produced using NDVI from the SY_2_V10 product at 1-km ~~grid scale, by averaging the 100-m SM estimation within each 1-km grid cell, to obtain the 1-km SM product using the same 1-km grid extent of the $CoperSSM$ product . In the second version of the S^2MP algorithm, the~~ resolution from S3 (see Sect. 2.1.3). Due to the spatial resolution of the S3 NDVI~~was used instead of the S2 NDVI. In this case~~, the S1 ~~VV backscattering and the incidence angle at each S1 acquisition were averaged directly at~~ backscattering signal and incidence angle were first aggregated from 10-m to 100-m resolution and then re-aggregated from 100-m to 1-km ~~scale only for~~ only over croplands and herbaceous vegetation~~areas inside each 1-km grid cell and the NDVI values were derived directly from the S3 images at 1-km scale. The SM estimation using~~ . Then, the neural network ~~inversion was thus directly applied at~~ was only applied over 1-km~~grid scale to obtain 1-km SM estimations~~^{2} pixels that are partly or entirely covered by croplands and/or herbaceous vegetation. The objective was to assess the impact of using lower spatial resolution NDVI as inputs to the S^2MP algorithm.

3.2 ~~Data sets comparisons and evaluations~~

~~Comparisons between data sets and evaluations against in situ measurementswere done from January 2017~~ Hereafter S^2MP_{S1S2} and S^2MP_{S1S3} will refer to the S^2MP SM datasets derived based of the synergistic use of S1 + S2, and S1 + S3 measurements, respectively. S^2MP_{S1S2} and S^2MP_{S1S3} were produced from January to December 2019. ~~Only ascending orbits from SMOS and descending orbits from SMAP within this time period were considered.~~

~~Relative~~ Both for S^2MP_{S1S2} and S^2MP_{S1S3}, it is important to highlight again that there is no SM estimate available over 1-km^2 pixels not covered at all by croplands and herbaceous vegetation. However, as long as there is a fraction of croplands and/or herbaceous vegetation (whatever the amount) within the pixel, SM values are provided. The proportion of croplands and herbaceous vegetation within each 1-km^2 pixel for the 6 regions of study is shown on the panel C from Figure 1.

3.2 CoperSSM and CoperSWI rescaling

Relative SM indices from $CoperSSM$ and $CoperSWI$ were scaled against ~~in situ data,~~ in-situ measurements for each region independently. This process is needed to transform the indices into SM ~~values~~ estimates with volumetric units ($m^3\ m^{-3}$). The following scaling formula was applied:

$$SM_n^* = SM_n \times [max(SM_n^{IS}) - min(SM_n^{IS})] + min(SM_n^{IS}) \quad (1)$$

where SM_n and SM_n^* are respectively the original and scaled SM ~~values~~ indices from $CoperSSM$. SM_n^{IS} ~~include~~ includes all the SM ~~observations~~ measurements from all the ~~in situ~~ in-situ time series available for the current region n ~~. The~~ in 2019 (Table 1). This concretely means 19 in-situ time series for the Spanish region, 4 in the southwest of France, 5 in the southeast of France, 11 for the Australian region, 26 in North America, and 5 in Tunisia.

The 2.5% lowest and 2.5% highest values are discarded before applying the minimum and maximum functions to remove the effect of possible outliers that can be caused by instrumental noise (Brocca et al., 2011). The same process was also undertaken to scale the SWI values from $CoperSWI$. The Copernicus indices were also scaled using $SMOSL3$ or $SMAPL3$ to obtain the maximum and minimum references instead of ~~in situ data~~in-situ measurements. The final results were quite comparable regardless the reference used and thus only the scaling against ~~in situ~~ in-situ measurements was used for the rest of the study.

~~Since all the HR data sets are sampled on the same 1-km regular grid, the different time series~~

3.3 Datasets comparisons

Comparisons between datasets and evaluations against in-situ measurements were done from January to December 2019. In a first step, the S^2MP_{S1S2} and S^2MP_{S1S3} maps were compared on a per pixel basis for each region in terms of Pearson correlation (R), bias and standard deviation of the difference ($STDD$, also referred to as unbiased Root Mean Square of the Difference by some authors)~~creating maps of each metric. The results were analyzed as a function of the land cover class. More precisely, S^2MP_{S1S2}~~. The metrics for which the P-value exceeded the threshold of 5% (interval of confidence of 95%) were discarded.

In a second step, S^2MP_{S1S3} were compared to the 3 HR datasets described in Section 2: $CoperSSM$, $CoperSWI$ and $SMAPS1$. ~~Of course, the S^2MP_{S1S3} maps were also compared to those of S^2MP_{S1S2}.~~ This analysis was also performed by computing R, bias and $STDD$ on a per pixel basis for each region (all the HR datasets are sampled on the same 1-km regular grid). In addition, the metrics were analysed as a function of croplands and herbaceous vegetation coverage over 1-km^2 pixels. The metrics for which the P-value exceeded the threshold of 5% were discarded.

~~Finally~~In a third step, all the different CR and HR ~~data sets~~ datasets were evaluated against the ~~in situ data~~ in-situ measurements available in the 6 regions of study. To perform the analysis in the optimal conditions, only morning orbits from SMOS (ascending overpasses) and SMAP (descending overpasses) within this time period were considered. During the night and early in the morning, the soil is in thermal balance, meaning that the vegetation temperature is equal to the soil temperature. During the afternoon, the balance is lost and the vegetation temperature is closer to the air temperature leading to satellite

estimates of lower quality. This is often reflected by lower performances against in-situ measurements for the afternoon SM estimates than those of the morning (Leroux et al., 2014). For each ground station, the closest time series ~~of~~ from each remotely sensed ~~data set~~ dataset was compared to the ~~in situ~~ in-situ measurements by computing ~~the correlation~~ R, bias and $STDD$. Only samples for which the difference in acquisition times with the ~~in situ~~ in-situ measurements does not exceed 1 hour were taken into account to compute those statistical metrics. ~~Then, only in situ~~ Metrics for which the corresponding P-value exceeded the threshold value of 5% were discarded. This implies that only in-situ locations where all the ~~data sets provide a time series were used (Tab.~~ comparisons between the remotely sensed and in-situ time series showing significant metrics were considered for the assessment (Table 1). ~~Time series of~~ This concretely means 13 in-situ time series for the Spanish region, 3 in the southwest of France, 0 in the southeast of France, 10 for the Australian region, 15 in North America, and 2 in Tunisia.

Then, remotely sensed time series of anomalies in a 35-days time window were also compared to those of the in-situ measurements in terms of R. They were derived as follows.

$$SM_t^a = (SM_t - \mu_t)/\sigma_t$$

$$\mu_t = 1/N \times \sum_{n=t_1}^{t_2} SM_n \tag{2}$$

$$\sigma_t = \sqrt{1/(N-1) \times \sum_{n=t_1}^{t_2} (SM_n - \mu)^2}$$

where SM_t^a and SM_t are the SM and anomalies values at time t, respectively. N is the number of observations from t minus 17 days (t_1) to t plus 17 days (t_2).

Finally, the HR ~~data were also evaluated against in situ measurements~~ datasets (S^2MP_{S1S2}, S^2MP_{S1S3}, $CoperSSM$, $CoperSWI$ and $SMAPS1$) were evaluated against in-situ measurements (R, bias and $STDD$ with P-values below 5%) after aggregation at ~~a~~ 25-km resolution (same grid as that of $CCISM$) in order to compare their performances to the CR data at a comparable resolution.

4 Results

4.1 Sentinel-3 versus Sentinel-2 NDVI

~~The~~ S2 and S3 NDVI were compared in each ~~site at 1 km grid scale to help better understand the reliability of using the S3 NDVI instead of the S2 NDVI when estimating the SM at 1 km grid scale using the S^2MP algorithm. The S2 NDVI at 1 km grid scale was calculated by averaging the S2 NDVI pixels at 10 m scale corresponding to the cropland and herbaceous vegetation within each 1 km grid cell (same grid of the S3 NDVI) and compared to the S3 NDVI obtained at 1 km. Figure 2 shows scatter plots between the S2-NDVI and the S3-NDVI over the year 2019 for all the study sites. Figure 2shows that the correlation between the S2-NDVI and the S3-NDVI varies across the studied sites with high correlations~~ region of study at 1-km grid scale in terms of R^2 as scatter plots in Figure 2. High R^2 are observed in Australia (0.86) and Tunisia (0.79), ~~moderate correlations for both USA~~ and moderate values are found in North America (0.68) and Spain (0.64)~~and no correlation~~

~~in the west and east of Occitanie.~~ . No significant correlation is observed in the southwest and southeast of France The results indicate that in dry regions such as ~~that~~ in Australia, Tunisia and ~~USA~~ North America, high correlation exists between S2 and S3 NDVI whereas low correlation ~~between S2 and S3 NDVI~~ is present in ~~humid areas such as the Occitanie region. The results also show that the S3-NDVI for all sites saturates at approximately~~ temperate areas with patchy land covers such as in the south of France. For all the study regions, S3 NDVI saturates between 0.6 and 0.7 whereas ~~the S2-NDVI~~ S2 NDVI reaches higher values between 0.8 and 0.9. The ~~lower NDVI values provided by S3 NDVI compared to the S2 NDVI~~ difference could be mainly due to the mixture of ~~the surface reflectance for~~ surface reflectances from different land cover classes ~~in the 1 km S3-NDVI.~~ within the 1-km S3 NDVI.

Figure 3 shows the distribution of ~~the correlation coefficient (R2) values for each site~~ R^2 between S2 and S3 NDVI as a function of the months ~~. The results show that in the dry periods of the year (summer season of each site) , the correlation between the S2 and S3 NDVI is higher than that in the~~ for each region. In general, higher correlations are obtained in the summer season (dry periods) than in winter and spring ~~season~~(humid periods). For example, ~~the Australian site shows that the correlation between the S2-NDVI and the S3-NDVI~~ R^2 between S2 and S3 NDVI is only high (0.72) ~~in the~~ from January to June (summer and autumn ~~season between January and June. In USA, months~~ seasons) in Australia. In North America, from March to July~~had a correlation~~ , R^2 is between 0.25 and 0.53 whereas ~~other months had no correlation between the~~ no significant correlation between S2 and S3 NDVI ~~values. In Occitanie east and west,~~ is found for the others months. In the southwest and southeast of France, no correlation are found for most of the months ~~show no correlation between the S2 and S3 NDVI values except for some summer months such as~~ except in summer such as in June, July and August. ~~In fact, winter and spring seasons encounters~~ On the one hand, the highest NDVI values are found in winter and spring seasons due to the development of the vegetation cycles. On the other hand, summer seasons usually ~~have low NDVI values corresponding~~ show lower NDVI values that corresponds to bare soil conditions except in the presence of irrigated summer crops. Thus, S2 and S3 NDVI are highly correlated for low NDVI values (usually in summer)~~the S2 and S3 are highly correlated whereas~~ . However, the correlation decreases for high NDVI values ~~with~~ because of the peak of the vegetation development (in spring)~~the correlation between S2 and S3 decreases~~.

4.2 ~~Comparison between S^2MP_{S1S2} and~~ S^2MP_{S1S3} comparison to S^2MP_{S1S2}

Figure 4 shows ~~the Pearson correlation (R)~~, bias and ~~standard deviation of the difference (~~$STDD$ ~~) between the~~ between S^2MP_{S1S2} and S^2MP_{S1S3} ~~maps~~for the 6 study regions. A very good agreement between the two ~~data sets~~ datasets was found in ~~the six~~ all the regions with $R \geq 0.9$, bias ≤ 0.04 $m^3\,m^{-3}$ (S^2MP_{S1S3} minus S^2MP_{S1S2}) and $STDD \leq 0.03$ $m^3\,m^{-3}$ for most of the areas. However, some differences in terms of bias can be seen between the two ~~data sets~~ datasets in the northwest of the Spanish region (Fig 4c), in the areas with significant forests cover in the France southwest region (Fig 4i) and in narrow areas of the Tunisian region ~~.~~ (Fig 4f).

The somewhat higher differences in the Spanish and France southwest regions are seen over pixels covered by ~~a mix of forests,~~ forests with a small fraction of croplands and herbaceous vegetation (~~dominated by forests), while the~~ see the Spanish

region in panels B and C from Fig. 1). The somewhat larger differences in some narrow areas of Tunisia is due to heterogeneous land cover around several river basins with rolling topography, sparse forests as well as grasslands.

As discussed above, these small differences ~~are~~ were expected due to the ~~use of~~ differences seen between S3 ~~NDVI estimated at 1-km resolution instead of~~ and S2 NDVI ~~at 100-m resolution, which are then aggregated only for croplands and herbaceous vegetation areas within the 1-km^2 pixels.~~ (Sect. 4.1) and the different way of aggregating the S1 backscatter coefficients (Sect. 3.1). However, taking into account the overall very good agreement ~~of~~ between S^2MP_{S1S2} and S^2MP_{S1S3} ~~maps~~, for the sake of simplicity and clarity, in ~~the following sections only S^2MP_{S1S2}~~ Section 4.3 only S^2MP_{S1S3} is compared to the other HR ~~data sets~~datasets.

4.3 ~~Comparison~~ General comparison of ~~S^2MP_{S1S2}~~ S^2MP_{S1S3} against the HR SM ~~data sets~~datasets

Figures 5, 6 and 7 present the comparison of ~~S^2MP_{S1S2}~~ S^2MP_{S1S3} against $CoperSSM$, $CoperSWI$ as well as $SMAPS1$ over the ~~six~~ 6 study regions in terms of bias, ~~standard deviation of the difference ($STDD$), and Pearson correlation (~~and R~~)~~, respectively. Some diagonal structures can be seen in the maps comparing ~~S^2MP_{S1S2}~~ S^2MP_{S1S3} to $CoperSSM$ in Spain and in the southwest of France. These artifacts, most pronounced in the ~~Pearson~~ correlation maps but also present in the bias and $STDD$ maps, come from the $CoperSSM$ data as previously discussed by Bazzi et al. (2019). Indeed, the artifacts are seen on the sub-swaths of the S1 product showing a big difference between the SM estimations in the $CoperSSM$ at the same SM estimation date. Bazzi et al. (2019) showed that the difference of the SM estimation at both sides of the sub-swath at a given date of the $CoperSSM$ map can reach 0.11 m^3m^{-3}.

4.3.1 ~~Absolute values~~Comparison of the order of magnitude

~~Figure 5 shows that S^2MP_{S1S2} show~~ According to Figure 5, S^2MP_{S1S3} shows a bias in the range from -0.1 to 0.1 $m^3\,m^{-3}$ with respect to the other HR products over most of the pixels within the ~~six~~ 6 regions of study. However, there are areas in the Spanish, Tunisian and France ~~south-east~~ southeast domains, where ~~S^2MP_{S1S2}~~ S^2MP_{S1S3} shows a dry bias of absolute value larger than 0.1 $m^3\,m^{-3}$. This is also particularly the case in the southwest of France, with respect to $CoperSSM$ and $CoperSWI$ as well as with respect to $SMAPS1$ in Australia and North America. For these regions and HR ~~data sets~~datasets, the bias is negative over the whole area. For all the other combinations of regions and HR products, the bias values are both positive and negative. ~~For instance, the bias distribution of S^2MP_{S1S2} with respect to~~ In general, there is no clear relationship between the sign of the bias and the dominant land cover class. However, in the case of the comparison between S^2MP_{S1S3} and $SMAPS1$ in the France southwest region, the bias distribution is splitted in two (Fig. 5i). ~~The bias is wet~~ A wet bias is observed in the west part of the region ~~and dry~~ corresponding to forests areas with low fractions of croplands and herbaceous vegetation, while a dry bias is found in the east part ~~. There is no clear relationship between this behavior and the dominant land cover class. However~~corresponding to areas dominated by croplands (Panels B and C from Fig. 1). In addition, the dry bias observed in the east part of the Tunisian region corresponds to an area of salted lakes, named Sebkha, whose water and moisture contents can vary significantly according to climate.

Figure 6 shows that the $STDD$ values of ~~S^2MP_{S1S2}~~ S^2MP_{S1S3} with respect to $CoperSSM$ and $CoperSWI$ are lower than ~~0.05~~ 0.06 $m^3\ m^{-3}$ over almost all the pixels ~~of~~ within the 4 regions where the Copernicus ~~data sets~~ datasets are available. ~~However, the $STDD$ obtained with respect to $SMAPS1$ (Fig. 6c,i,l) are often much higher and can reach 0.12~~ Higher values close to 0.08-0.10 $m^3\ m^{-3}$ ~~. These significant differences are specifically observed in the west~~ between S^2MP_{S1S3} and $CoperSSM$ are found in the southwest part of the ~~Spanish region, the east part of the France southwest region as well as the northwest part of the Francesoutheast region~~southwest region of France. The $STDD$ obtained ~~in Tunisia with respect to~~ between S^2MP_{S1S3} and $SMAPS1$ ~~(Fig. 6f)~~ are comparable to those obtained with respect to the Copernicus ~~data sets (Fig. 6d, e) in the north~~ datasets. However, values reaching 0.08-0.12 $m^3\ m^{-3}$ are more often found, in particular in the west part of the ~~same~~ Spanish region, and ~~do not exceed 0.06 $m^3\ m^{-3}$.~~ sparsely in the southwest and southeast of France. In Australia and North America (Fig. 6m,n), the $STDD$ with respect to $SMAPS1$ are quite similar to those found in Spain, Tunisia and France (Fig. 6c,f,i,l), where values can reach ~~$\sim 0.08 - 0.1$~~ $\sim 0.08 - 0.12$ $m^3\ m^{-3}$ in the southeast and ~~northwest~~ west parts of the Australia and North America regions, respectively. There is no clear and unique relationship with the dominant land cover class. For instance, the $STDD$ with respect to $SMAPS1$ in the southwest of France is higher over the forests than over the croplands dominated areas, while in the North America region the $STDD$ was found to be lower over the ~~forest.~~ forests (see panels B and C from Fig. 1).

4.3.2 Comparison of the temporal dynamics

4.3.3 ~~Temporal dynamics~~

~~Overall, S^2MP_{S1S2}~~ Overall, S^2MP_{S1S3} and $CoperSSM$ show a high correlation (above 0.7-0.8) over almost all the pixels ~~for~~ within all the regions of study (Figs. 7a,d,g,j). In contrast, lower values are found for the correlation between ~~S^2MP_{S1S2}~~ S^2MP_{S1S3} and $CoperSWI$ (~~maximum values of 0.6-0.7 and values lower than 0.4 in many large areas,~~ Figs. 7b,e,h,k) ~~. Finally, the lowest correlation values are obtained with respect to the~~ as well as between S^2MP_{S1S3} and $SMAPS1$ ~~data set~~ (Figs. 7c,f,i,l,m,n). R rarely exceed 0.7 and values lower than 0.6 are observed in many large areas.

In the Spanish region, the highest ~~correlation~~ R values are obtained in the areas dominated by croplands. The lowest values are found in the northwest ~~and in a few spots in the south and the center of the region. In all cases, those are areas with heterogeneous land cover~~ over heterogeneous pixels dominated by forests ~~.~~ (Panels B and C from Fig. 1). Similar spatial features are observed in the ~~three maps comparing S^2MP_{S1S2}~~ 3 maps comparing S^2MP_{S1S3} to $CoperSSM$, $CoperSWI$ and $SMAPS1$ (Figs. 7~~a-c)but with lower values of correlation~~ a,b,c). However, lower R values are found with respect to ~~$CoperSWI$. The areas of high correlation with respect to~~ $SMAPS1$ ~~show higher values than with respect to~~ and $CoperSWI$~~but the areas with low correlation also show lower values than with respect to~~ . In addition, the comparison against $CoperSWI$ ~~.~~ shows R below 0.5 in a few spots in the south and the center of the region.

In Tunisia (Fig. 7d-f), the ~~correlations~~ correlation values obtained in the north are quite good with values of 0.8-0.9 with respect to $CoperSSM$~~and 0.6-0.7 with respect to $SMAPS1$. The values~~ . R drop in the ~~south~~ southeast and southwest to values lower than ~~0.3, especially near the~~ 0.5. The decrease in the southwest can be partly explained by the proximity of coasts,

where mixed land cover pixels include urban areas . (Panel B from Fig. 1). The correlation with respect to $CoperSWI$ (Fig. 7e) is only higher than 0.5 for the regions where the 1-km^2 pixels are dominated by croplands(. The comparison between S^2MP_{S1S3} and $SMAPS1$ results in a large range of correlations. Only the very north areas dominated by croplands show correlations above 0.6 (Panels B and C from Fig. 1). R close to 0.4-0.5 are found in the east and west parts of the region. Values lower than 0.2 are observed in the center of the region over heterogeneous pixels around several river basins that were also highlighted in Section 4.2 with Figure 4f.

In the France southwest region (Fig. 7g-i), there is a clear frontier from the areas where the pixels are the distribution of R is quite homogeneous over the whole area and does not vary significantly according to pixels dominated by croplands with respect to the areas dominated or by forests (Panel B from Fig. 1). In the case of the correlation R values with respect to $CoperSSM$, values remain higher than 0.7 for are mainly above 0.8 over most of the areas dominated by forests. However in the case of the correlation pixels while the values drop to 0.5 with respect to $CoperSWI$. The comparison between S^2MP_{S1S3} and $SMAPS1$, values in those areas decrease to lower than 0.3. In shows R closer to 0.6 in general but really low correlation values (below 0.2) appear over several pixels. The same pattern is observed in the France southeast region (Fig. 7j-l), but correlations are only significant with respect to $CoperSSM$ and in regions over areas dominated by croplands.

The correlations between S^2MP_{S1S2}

R between S^2MP_{S1S3} and $SMAPS1$ reach 0.6-0.7 in Australia 0.7-0.8 in Australia and North America (Fig. 7m). Similar moderate to low correlation values are obtained in North America ,n) with no clear relationship with the land cover type(Fig. 7n). .

4.3.3 Comparison over areas dominated by croplands and herbaceous vegetation

4.3.4 Comparison as a function of land cover

As discussed above, the correlation maps show some features related to the dominant land cover class, in particular, higher correlations are found for areas dominated by croplands and herbaceous vegetation.

To get further insight into the effect of the dominant land cover analysis over croplands and herbaceous vegetation, S^2MP_{S1S3} was exclusively compared to $CoperSSM$, $CoperSWI$ and the homogeneity of the land coverwithin the 1-km^2 pixels, Table 2 gives the median Pearson correlation $SMAPS1$ over pixels where one of these two land cover classes is dominant. For each region and land cover, a set of metrics (R) of S^2MP_{S1S2} with respect to $CoperSSM$, $CoperSWI$ and $SMAPS1$ for pixels dominated by , bias and $STDD$) is computed in two ways. One set is computed by only taking into account pixels covered by less than 75% of croplands or herbaceous vegetation. The other set is computed by only taking into account pixels covered by at least 75% of croplands and herbaceous vegetationto different extend: *(i)* "mixed" pixels in which croplands or herbaceous vegetationare the dominant land cover class in any proportion and *(ii)* "homogeneous" pixels in which croplands or herbaceous vegetation represent at least . The results are summed up in Table 2.

Over pixels in Europe (Spain, Tunisia, France) where croplands represent less than 75% of the 1-km^2 area.

~~In the Spanish region, S^2MP_{S1S2}~~ area, S^2MP_{S1S3} is better correlated to $CoperSSM$ ~~($R \sim 0.7$-0.8)~~ than $CoperSWI$ ~~($\sim$ 0.55-0.65)~~and $SMAPS1$~~($R \sim 0.45$-0.65) when pixels become more homogeneous. The same pattern can be observed in~~ . In general, high R values are found in Spain (0.54-0.63), moderate values (0.28-0.63) are observed in France and low values are found in Tunisia (0.37-0.38). In addition, R values obtained in Australia and North America with respect to $SMAPS1$ are comparable to those found in Spain. Absolute bias between S^2MP_{S1S3} and the 3 HR datasets in Spain (0.01 $m^3\,m^{-3}$) are lower or similar to those found in the other regions. The strongest absolute bias is observed in North America with respect to $SMAPS1$ with 0.07 $m^3\,m^{-3}$. According to the $STDD$ values, no particular trend is observed over the ~~southwest and southeast of France when S^2MP_{S1S2} is compared to~~ 6 regions of study and values range from 0.04 to 0.09 $m^3\,m^{-3}$. For most of the regions and comparisons, the correlation values significantly increase (+ 0.05-0.1) over pixels that contain at least 75% of croplands. In overall, absolute bias and $STDD$ values remain similar but sometimes there is a slight decrease (-0.01 $m^3\,m^{-3}$).

Taking into account pixels where herbaceous vegetation represent less than 75% of the area, S^2MP_{S1S3} is only better correlated to $CoperSSM$ ~~and $CoperSWI$ over croplands. Correlations between S^2MP_{S1S2} and $SMAPS1$ significantly drop in those regions ($R \sim 0.2$-0.5) over croplands as well as herbaceous vegetation areas. In addition, S^2MP_{S1S2} shows very low correlations with respect to the other SM HR data sets~~ in Spain and the southwest of France. In general, high R values are found in Spain (0.64-0.67), moderate values (0.36-0.69) are observed in France and low values are found in Tunisia (~~$R \sim$ 0.2-0.55)for the both land cover types. However, the correlations obtained between S^2MP_{S1S2} and $SMAPS1$~~ 0.32-0.36). In addition, R values obtained in Australia and North America ~~($R \sim 0.5$-0.55) are higher than~~ with respect to $SMAPS1$ are comparable to those found in the southwest of France. Absolute bias between S^2MP_{S1S3} and the 3 HR datasets in Tunisia (0.01-0.02 $m^3\,m^{-3}$) are lower or similar to those found in ~~France~~ the other regions. The strongest absolute biases are observed in the southwest of France with 0.09 $m^3\,m^{-3}$ for $CoperSWI$ and $SMAPS1$, respectively. The $STDD$ is higher with respect to $SMAPS1$ and can reach 0.07, 0.08 and ~~Tunisia, both over croplands and herbaceous vegetation.~~

~~Compared to the other HR data sets, S^2MP_{S1S2} shows generally higher correlations over croplandsthan over~~ 0.10 $m^3\,m^{-3}$ in Tunisia, Spain, and in the southwest of France, respectively. In contrast with croplands, the correlation values does not systematically increase over pixels that contain at least 75% of herbaceous vegetation. ~~In addition, there is a clear improvement in correlation of S^2MP_{S1S2}~~ There is no significant change concerning the $STDD$ and in overall the absolute bias increases with respect to ~~the other data sets when the land cover within the pixel is homogeneous, in particular over croplands .~~ almost all the HR datasets (+0.01-0.04 $^3\,m^{-3}$).

It is noteworthy that the bias is significantly higher over herbaceous vegetation than over croplands in Spain and in the southwest of France, while the $STDD$ is quite similar regardless the region of study. In addition, higher R values are found over herbaceous vegetation in Spain. In Tunisia, the correlation and absolute bias values are among the lowest both over croplands and herbaceous vegetation. Low absolute biases can be partly explained by the fact that the region is really dry with desert areas implying a small SM dynamic range with very low values regardless the estimation algorithm used.

4.4 Evaluation against ~~in situ data~~in-situ measurements

Table 3 presents the evaluation of the different CR and HR SM products with respect to ~~in situ data in~~ in-situ measurements in terms of bias, $STDD$ and ~~Pearson correlation~~ R ~~(R)~~ of the original time series (R^a). ~~The highest bias is obtained for $CCISM$ with 0.07~~ In addition, Figure 8 shows examples of time series of the different HR and CR datasets at 6 in-situ stations used in this study (one for each region).

The highest absolute biases with respect to in-situ measurements are obtained for S^2MP_{S1S2} and S^2MP_{S1S3} with -0.06 $m^3\ m^{-3}$~~. The SMAP products, S^2MP_{S1S2} as well as~~, closely followed by $CoperSWI$ with 0.05 $m^3\ m^{-3}$. $SMOSNRT$, $SMOSL3$, $CCISM$ and $SMAPS1$ show the lowest ~~bias ($\leq$ 0.005~~ absolute biases with 0.03 $m^3\ m^{-3}$~~in absolute value) with respect to in situ data.~~ .

The highest $STDD$ with respect to in-situ measurements are obtained for $CoperSSM$ (0.08 $m^3\ m^{-3}$) and ~~lowest $STDD$ (0.04~~ $SMOSL3$ (0.07 $m^3\ m^{-3}$)~~are obtained for $CoperSSM$ and $CCISM$, respectively. S^2MP_{S1S2}, as most of the data sets, shows an in between value~~ . The other datasets shows comparable $STDD$ with 0.05 or 0.06 $m^3\ m^{-3}$.

~~The highest~~ In general, higher correlation values are obtained for the ~~coarse resolution data (0.65-0.68) and the lowest for the S^2MP_{S1S2} and $CoperSSM$ Sentinel-only HR data sets (0.44-0.48~~CR data (0.67-0.77) than for the HR data (0.53-0.74). The ~~HR~~ lowest correlations are found for the Sentinel-only HR datasets with 0.53 for $CoperSSM$, 0.56 for S^2MP_{S1S3} and 0.59 for S^2MP_{S1S2}. Concerning the HR data obtained from merging approaches~~(~~, $SMAPS1$ still shows a value lower than the CR datasets with 0.64 but $CoperSWI$ shows the third best value with 0.74, just after $SMAPL3E$ (0.77) and ~~$SMAPS1$~~$SMAPL3$ (0.76)~~show intermediate values (0.60-0.64)~~.

Regarding the correlation of the anomalies time series, ~~$CoperSWI$ gets~~ $SMAPL3E$ and $SMAPL3$ get the highest R^a with respect to ~~in situ data with 0.49, closely followed by $SMAPL3E$ with 0.46~~in-situ measurements with 0.59 and 0.58. $CoperSSM$~~and~~ , S^2MP_{S1S2}, $SMAPS1$, and S^2MP_{S1S3} show the lowest ~~performances with~~ R^a ~~equal to 0.25 and 0.26. S^2MP_{S1S2} gets a higher value with~~ with 0.18, 0.36~~, which is also better than two CR data sets: $SMOSL3$ ($R^a \sim 0.30$) and $SMOSNRT$ ($R^a \sim 0.33$).~~ , 0.35 and 0.37 respectively.

The CR time series have a temporal revisit roughly five times higher than those from S^2MP_{S1S2}, S^2MP_{S1S3}, $CoperSSM$ and $SMAPS1$ (Fig. 8). In order to understand if the low temporal revisit of the HR data affects their performances against in-situ measurements, one observation out of five was removed from the CR time series and the metrics were re-computed (not presented). However, no significant differences in terms of R, bias and $STDD$ were found.

The performances of the two Sentinel-only HR ~~data sets~~ datasets averaged at 25-km resolution ($S^2MP^*_{S1S2}$, $S^2MP^*_{S1S3}$, $CoperSSM^*$) with respect to ~~in situ data~~ in-situ measurements are comparable to the performances obtained for the original 1-km ~~data sets. The performance of the merged ASCAT+S1 (~~datasets (S^2MP_{S1S2}, S^2MP_{S1S3}, $CoperSSM$, $CoperSWI^*$)~~averaged at 25-km resolution is also similar to that of the 1-km resolution data set ($CoperSWI$).~~ . In contrast, for the $SMAPS1^*$ ~~data set~~dataset, which is a downscaled product, the correlation increases from ~~0.60~~ 0.64 at 1-km resolution ($SMAPS1$) to ~~0.69~~ 0.79 at 25-km resolution~~.~~ , which is the highest correlation found among all the datasets. In addition, the $STDD$ and bias

slightly decrease. R^a also increases from ~~0.26~~ 0.35 at 1-km resolution to ~~0.32~~ 0.44 at 25-km resolution, but it does not reach the values of R^a obtained for the SMAP-only products ($SMAPL3$ and $SMAPL3E$ ~~) products (0.43-0.46)~~with 0.58-0.59).

5 Discussion

~~The four HR data sets evaluated in this study have been~~ S^2MP, S^2MP_{S1S3}, $CoperSSM$, $CoperSWI$ and $SMAPS1$ are all HR datasets that were produced with different approaches. Two products were obtained by merging S1 data with ASCAT ($CoperSWI$) and SMAP ($SMAPS1$), respectively. ~~S^2MP_{S1S2}~~ S^2MP and $CoperSSM$ are based on Sentinel-only. The last one is computed from local temporal variations of the S1 backscatter coefficients time series following the method of Wagner (1998). In contrast, ~~S^2MP_{S1S2} uses electromagnetic modelling to compute a database predicting backscatter coefficients from~~ S^2MP provides SM estimates derived from a NN that uses a database gathering backscatter coefficients and HR NDVI from Sentinel as inputs. The NN was initially trained on a synthetic database containing backscatter coefficients and surface characteristics such as SM and vegetation status (approximated by NDVI) ~~. This database is in turn used to train a neural network to predict SM from S1 backscatter coefficients and HR NDVI estimations.~~ that were predicted from electromagnetic modelling.

Initially, the S^2MP algorithm by El Hajj et al. (2017) was ~~limited to croplands and the use of~~ only providing SM estimates over croplands at 10-m resolution using NDVI derived from S2 optical images. In the framework of this study, the algorithm has been extended to provide SM estimates at 1-km resolution also over herbaceous vegetation areas. ~~In addition, two methodologies are used to mimic vegetation dynamics. In the first approach,~~ and S2 was replaced by S3. However, despite the different ways of aggregating the S1 ~~backscatter coefficients and~~ radar signal and the differences between S3 and S2 NDVI ~~are estimated over croplands and herbaceous vegetation areas at a 100-m resolution and then they are aggregated within 1-km^2 pixels (~~(Sect. 4.1 with Figs. 3 and 2), S^2MP_{S1S2} ~~). In the second approach, instead of using S2 NDVI, S3 NDVI are obtained directly at a resolution of 1 km (S^2MP_{S1S3}).~~

~~The results of this study show that when the target resolution is 1 km,~~ and S^2MP_{S1S3} are in very good agreement over the 6 study regions (Sect. 4.2 with Fig. 4). Thus, these results imply that it is possible to replace S2 ~~NDVI~~ by S3 ~~NDVI~~ in the S^2MP approach without losing skill. ~~Regarding the comparison to~~ In addition, although the higher temporal revisit of S3 compared to S2 does not allow the S^2MP algorithm to provide SM estimates more frequently because the effective revisit is that of S1 (see Fig. 8), the production of the SM daily maps using S3 instead of S2 is easier and faster. S2 and S3 NDVI are derived from optical measurements remotely sensed from space that are highly dependent on the cloud cover situation. Both S2 or S3 NDVI can be unreliable during long rainy or cloudy periods ($>$ 15 days) over specific regions. However, the higher temporal revisit of S3 allows the instruments onboard S3 to retrieve more optical images without cloud conditions than those onboard S2. This results in a better estimation of the vegetation cycle through the NDVI computation. Finally, less processing steps are required thanks to the availability of NDVI estimates already provided in the 1-km VEGETATION-like product from Copernicus (see Sec. 2.1.3).

According to Bazzi et al. (2019), the ~~other Sentinel-only product ($CoperSSM$), high correlations have been found over croplands and herbaceous areas (Tab. 2) . Different SM dynamics are actually noticeable, e. g. , in the forested areas of southwestern France (Fig. 1 and 7).~~ S^2MP algorithm tends to provide unreliable SM estimates when the NDVI used exceeds 0.7. NDVI above this value correspond to well-developed vegetation and even if it is more common to have NDVI lower than 0.7 with S3 than with S2 (Figure 2) due to averaging effets, using S3 NDVI does not solve the problem. Indeed, in the particular cases of well-developed vegetation, the problem does not arise from the S2 of S3 NDVI itself, but from the C-band SAR signal which fails to penetrate the vegetation cover.

~~In addition, slightly better results of S^2MP_{S1S2} with respect to in situ measurements compared to~~

Regarding the comparisons between the HR datasets carried in Section 4.3, S^2MP_{S1S3} shows a temporal dynamic closer to those of $CoperSSM$ ~~were found (Table 3). This is also true for the bias even if the~~ , $CoperSWI$ and $SMAPS1$ over semi-dry areas such as in Spain, North America and Australia. However, the correlation drops significantly over very dry zones (Tunisia). Over semi-humid areas (France), the temporal dynamic between S^2MP_{S1S3} and $CoperSSM$ ~~retrievals have previously been scaled against the in situ data. Most of the ground sites are representative of croplands and herbaceous regions. Therefore~~is in better agreement than with respect to $CoperSWI$ and $SMAPS1$. The order of magnitude (bias and $STDD$) between S^2MP_{S1S3} and the other HR datasets is quite similar regardless the study region, the land cover as well as the climate zone (rather dry or humid). In addition, it is ~~difficult to evaluate the relative performance against in situ measurements over~~ noteworthy to highlight that differences in terms of bias and $STDD$ are not systematically reduced over homogeneous pixels covered by croplands or herbaceous vegetation. It means that inherent biases exist between the algorithms and they might persist over other land cover ~~types for which more differences would be expected, e. g., forest cover. On the one hand~~classes such as over forests (if the S^2MP approach is extended to forests).

At the moment, by construction, the S^2MP algorithm starts being out of its application domain when considering pixels dominated by forests cover. ~~On the other hand, the~~ This is also the case for the change detection approach use to produce $CoperSSM$. Indeed, the SM indices computation does currently not account for vegetation dynamics, which can lead to biases ~~with respect to in situ data~~ over areas covered by seasonal and dense vegetation. In addition, for most applications the $CoperSSM$ indices ~~should also~~ as well as those from $CoperSWI$ should be transformed into SM time series and this will be problematic without reference SM values under forest to scale them. Therefore, an extension of the S^2MP ~~approach~~ algorithm to forest areas would definitely be interesting to provide HR SM mapping over large regions inside and outside Europe.

~~SM retrievals~~ In this study, most of the SM measurements used from the ground stations were representative of croplands and herbaceous regions. Hence, the relative performances of the HR datasets (S^2MP, $CoperSSM$, $CoperSWI$, $SMAPS1$) were not assessed over dense vegetation areas.

In addition, slightly better results of S^2MP_{S1S3} with respect to in-situ measurements compared to those of $CoperSSM$ were found, except for the bias (Table 3).

SM estimates using the S^2MP ~~approach~~ algorithm were already evaluated against ~~in situ~~ in-situ measurements along with other HR and CR ~~data sets~~ datasets by El Hajj et al. (2018) and ~~compared to CGLS SM~~ by Bazzi et al. (2019). In ~~their evaluation with respect to in situ data, El Hajj et al. (2018)found that the~~ El Hajj et al. (2018), the authors found that

S^2MP_{S1S2} ~~data set shows lower correlations~~ shows lower correlation with respect to in-situ measurements than $SMAPL3$ and $SMAPL3E$ but higher ~~correlations~~ than $SMOSNRT$, $SMOSL3$ and $SMAPS1$. In contrast, in the current study, the S^2MP_{S1S2} shows a lower correlation against ~~in situ data than the other products. These differences can be due to the fact that the analysis was only carried out in the south of France during a different time period (from January 2016 to June 2017).~~ ~~Moreover~~in-situ measurements than all the other HR and CR products. However, in El Hajj et al. (2018), SM estimates from the S^2MP algorithm were only derived over croplands while in our study, the ~~S^2MP SM retrievals were performed both for~~ SM estimation was performed both over croplands and herbaceous vegetation. ~~However, the results of the current study are in good agreement with those of El Hajj et al. (2018) in terms of bias. In both studies, S^2MP_{S1S2} shows low bias compared to in situ measurements, similar to or lower than the CR data sets. Regarding the S^2MP_{S1S2} and $CoperSSM$ comparison by Bazzi et al. (2019), it is interesting to note~~ Moreover, their analysis was only carried out in the south of France during a different time period (from January 2016 to June 2017). In Bazzi et al. (2019), the authors found that S^2MP_{S1S2} is better correlated to ~~in situ data~~ in-situ measurements than $CoperSSM$~~, which is in agreement with~~ . According to the results of our study (Table 3)~~.~~ , higher correlations are also obtained for S^2MP_{S1S2}. In addition, it is interesting to note that S^2MP_{S1S2} and S^2MP_{S1S3} show similar performances with respect to in-situ measurements.

Taking into account the ~~results discussed in the previous section~~evaluations of all the HR and CR products together (Table 3), HR merged ~~products~~ datasets ($SMAPS1$, $CoperSWI$) provide better estimations or temporal agreement with ~~in situ data~~ respect to in-situ measurements than the HR Sentinel-only ~~data~~ ones (S^2MP_{S1S2}, S^2MP_{S1S3}, $CoperSSM$)~~(Tab. 3) but still show~~ . However, they still show similar or lower performances than the CR ~~data. This was also found by Bauer-Marschallinger et al. (2019) , who~~ datasets (Tab. 3). This can be partly explained by the fact that the HR datasets provide SM estimates using C-band measurements while the CR datasets used in this study are computed using L-band measurements. Indeed, SMOS and SMAP were specifically designed to measure surface SM, which was not the case for the Sentinel satellites. Regarding the higher performances of the CR datasets over the HR ones with respect to in-situ measurements, Bauer-Marschallinger et al. (2019) also demonstrated that 25-km resolution SM estimates from ASCAT were better correlated to ~~in situ~~ in-situ measurements within the Italian Umbria region that those of the 1-km resolution $CoperSSM$. The results of our study are also in perfect agreement with the findings by Ojha et al. (2021), who showed over several regions in France and Spain that two merged products, $SMAPS1$ and SMAP + DISPATCH (Merlin et al., 2012), were better correlated to ~~in situ data~~ in-situ measurements than $CoperSSM$~~over several regions in France and Spain.~~

~~When aggregated to CR,~~ . Finally, it is noteworthy that the performances of ~~the~~ $SMAPS1$ aggregated from 1-km ~~data~~ to 25-km resolution (CR) increase to values similar to those of ~~the~~ $SMAPL3$~~data~~. This implies that the gain in resolution brought by merging data of different resolutions comes at the expense of introducing uncertainties in the resulting HR ~~data set~~dataset.

Obviously, this study was limited to comparisons over ~~six~~ 6 regions of 10^4 km^2 within a ~~3-years~~ 1-year time period, so the results can not be straightforwardly extended to a global scale. However, ~~it is noticeable that the HR products provide SM estimates using C-band measurements while the CR data sets used in this study are computed using L-band measurements . Indeed, SMOS and SMAP were specifically designed to measure surface SM~~ the results of the study shows that the use of S3 NDVI as input to the S^2MP algorithm leads to SM estimates comparable to those obtained with S2 NDVI. Howevere, HR

SM estimates does not necessary lead to better performances with respect to in-situ measurements than CR SM estimates. In particular, retrieval algorithms only based on Sentinel measurements (S^2MP, ~~which was not the case for the Sentinel satellites.~~ $CoperSSM$) need improvements before reaching performances comparable to those used with the HR merged or CR datasets. However, the S^2MP datasets still have two advantages over $CoperSSM$. They currently show better performances against in-situ measurements and are able to provide SM estimates outside of Europe. Hence, it would be interesting to extend the S^2MP algorithm to all the types of land cover and to provide SM estimates over the entire Globe. The objective would be to produce the first Sentinel-only SM dataset available at global scale and to perform deeper comparisons against $SMAPS1$ over large areas. However, the estimation of SM using the S^2MP algorithm outside of Europe would remain challenging due to the in-homogeneous spatial and temporal coverage of S1 (Bauer-Marschallinger et al., 2019).

6 Conclusions

The goal of this study was to adapt the S^2MP approach, originally designed to retrieve SM at ~~the plot scale~~ 10-m resolution over agricultural fields, to a 1-km resolution, which allows to replace S2 by S3 ~~NDVI~~ and to significantly improve the NDVI temporal sampling. In addition, the approach was extended to herbaceous land cover areas ~~in addition to croplands~~ and tested in six regions over four continents to assess its performances beyond previous evaluations in Southern France.

~~Very~~ A very good agreement was found between the S1+~~S2~~ S3 and the S1+~~S3~~ S2 S^2MP maps ~~in terms of correlations~~ for the 6 regions ($R \geq 0.9$~~), bias (~~, bias $\leq 0.04\ m^3\,m^{-3}$~~) and standard deviation of the difference (~~, $STDD \leq 0.03\ m^3\,m^{-3}$) ~~for the 6 regions.~~ meaning that it is possible to replace S2 by S3 NDVI.

The S^2MP maps were then compared to those of the 1-km surface SM product provided by CGLS ($CoperSSM$), which is also a Sentinel-only based ~~data set~~dataset. In contrast to S^2MP, ~~the CGLS surface SM is a local index~~ $CoperSSM$ provides local indices of SM variations~~and for many applicationsit has~~. For many applications, they have to be scaled against a reference to transform the ~~variation index~~ variations to actual SM in volumetric units ($m^3\,m^{-3}$) before being used. Then, S^2MP was also compared to two HR merged ~~data sets,~~ datasets: (~~i~~~~the SWI~~) the SWI dataset from CGLS combining S1 and ASCAT measurements ($CoperSWI$) as well as (*ii*) the SMAP+S1 dataset. As for the surface SM ~~data set~~dataset, the SWI data had to be scaled into absolute SM values. CGLS products only provide ~~retrievals~~ estimates over the European continent and the Mediterranean basin.

~~The results showed that~~ Overall, the S^2MP ~~data set is well~~ dataset is better correlated to the 1-km surface SM product provided by CGLS ~~in large areas of the 6~~ over the 4 regions of study ~~:~~ in Europe ($R \sim$ 0.7-0.8~~. However, the correlations significantly drop in some areas of the 6 domains when the S^2MP maps are compared to those of the SWI product and those of SMAP+S1.~~). Over almost all the pixels within the 6 regions, the ~~standard deviation of the difference ($STDD$)~~ between S^2MP and the ~~CGLS products~~ other HR datasets are lower than 0.06 ~~$m^3\,m^{-3}$ while the values obtained with respect to SMAP+S1 can reach 0.1 $m^3\,m^{-3}$. Then~~$m^3\,m^{-3}$. In addition, the bias ~~between S^2MP and the other HR data sets~~ differ significantly inside a same region and can be strongly dry or wet ($\pm$ 0.1 $m^3\,m^{-3}$). The correlations between S^2MP and the other HR ~~data sets~~ datasets improve over croplands when the 1-km pixels ~~are~~ become homogeneous but a similar behaviour

was not ~~found for~~ clearly found for the other metrics ($STDD$ and bias) and over pixels where the dominant land cover class is herbaceous vegetation.

~~The HR products~~

The S^2MP datasets were also evaluated with respect to ~~in situ~~ in-situ measurements along with ~~coarser resolution data sets~~ the 3 other HR datasets as well as with coarser resolution datasets from SMOS, SMAP and ESA CCI. The coarse resolution (CR) products show higher correlations (~~0.65~~ 0.68 $\leq R \leq$ ~~0.68~~0.77) than the HR ~~data sets (0.44~~ datasets (0.54 $\leq R \leq$ ~~0.64~~0.74), and the HR merged ~~data sets~~ datasets showed higher correlations than the HR Sentinel-only ones. ~~However, as several SMAP and SMOS data sets, S^2MP also showed a very low~~ S^2MP_{S1S2} showed the highest bias with respect to ~~in situ measurements~~ in-situ measurements with -0.07 m^3m^{-3}. Finally, the $STDD$ differ according to the ~~data set~~ dataset as well as the spatial resolution and range from ~~0.04~~ 0.05 (with S^2MP_{S1S2} for example) to 0.08 m^3m^{-3} ~~for the ESA CCI product to the SWI product~~($CoperSWI$).

~~The~~ In general, these results show that the HR datasets only based on Sentinel (S^2MP and $CoperSSM$) are not as competitive as the other HR merged and CR datasets with respect to in-situ measurements in terms of correlation and bias, but S^2MP still presents several advantages. In contrast to the HR data from Copernicus, the S^2MP data do not depend on auxiliary data to be scaled into volumetric units and can provide SM estimates outside of Europe. S^2MP_{S1S2} also shows lower $STDD$ with respect to in-situ measurements than the Copernicus and the SMAP+S1 datasets. It would be interesting to extend the S^2MP ~~algorithm gave promising results over the 6 regions of study. Of course, for some applications the approach should be extended to consider other land cover types than croplands and herbaceous. For instance, a 1 km resolution SM data sets over all land cover types~~ to all the types of land cover and to provide SM maps at the globe scale. S^2MP_{S1S2} would be the first global SM dataset at 1-km resolution only based on Sentinel measurements. It would also allow to perform deeper comparisons against SMAP+S1 over large areas and S^2MP_{S1S2} could be used to ~~asses~~ assess climate impact at regional level in the future~~when 1 km SM times series are longer. Finally~~. However, a remaining challenge is to provide HR SM data with comparable spatio-temporal coverage and retrieval quality across different land cover types than those of the state-of-the-art coarse resolution products, such as the SMOS, SMAP and ESA CCI products.

Author contributions. RM, NJR-F, NB and MZ designed the study. RM and NJR-F undertook the different evaluations and wrote the first version of the manuscript. HB and NB produced the S^2MP_{S1S2} and S^2MP_{S1S3} maps. CA, NB, WD and MZ participated in the analysis of the results. All the authors contributed to the final version of the manuscript.

Competing interests. The authors declare no conflict of interest.

Acknowledgements. This research made use of data from the Centre Aval de Traitement des Données SMOS (CATDS) operated for the Centre National d'Etudes Spatiales (CNES) by The Institut Français de Recherche pour l'Exploitation de la Mer (IFREMER) in France, as well as from the Copernicus Global Land Service (CGLS), the National Snow and Ice Data Center (NSIDC)~~and~~ , the ESA's Climate Change Initiative for Soil Moisture project, the Centre d'Etudes Spatiales de la BIOsphère (CESBIO), the Institut National Agronomique de Tunisie (INAT) and the International Soil Moisture Network (ISMN). The authors acknowledge partial funding from the ESA's Climate Change Initiative for Soil Moisture project (Contract No. 4000104814/11/I-NB and 4000112226/14/I-NB). RM and NJR-F acknowledge partial funding by the Centre National d'Études Spatiales (CNES) APR TOSCA project SMOS-TE.

Table 1. In-situ measurements that were used in this study. The depths are quoted as two numbers: the first one is the upper depth, and the second one is the lower depth of the sensor. Both numbers are equal when the sensor is placed horizontally. The fourth column gives the number of sensors ~~available for each region~~that provide SM measurements in 2019. These measurements were used to convert the relative indices from $CoperSSM$ and $CoperSWI$ into SM estimates with volumetric units ($m^3\,m^{-3}$, Section 3.2). The number in parenthesis corresponds to the number of in-situ locations where the evaluations of the remotely sensed data were significant (P-value below 5%, Section 3.3).

~~Location~~ Measurements	Location	Depth (m)	Sensors	Reference
~~Spain~~ REMEDHUS	Spain	0–0.05	~~20~~ 19 (13)	Gonzalez-Zamora et al. (2018)
SMOSMANIA	Southwest of France	~~SMOSMANIA~~ 0.05–0.05	4 (3)	Calvet et al. (2007)
SMOSMANIA	Southeast of France	~~SMOSMANIA~~ 0.05–0.05	~~6~~ 5 (0)	Calvet et al. (2007)
~~Australia~~ OZNET	Australia	0–0.05	11 (10)	Smith et al. (2012); Young et al. (2008)
USCRN	North America	~~USCRN~~ 0.05–0.05	2 (1)	Bell et al. (2013)
~~Tunisia~~ ARM	North America	0.05–0.05	24 (13)	Cook (2016, 2018)
MERGUELLIL	Tunisia	0–0.05	~~6~~ 5 (2)	~~Gorrab et al. (2015)~~ ?Gorrab et al. (2015)

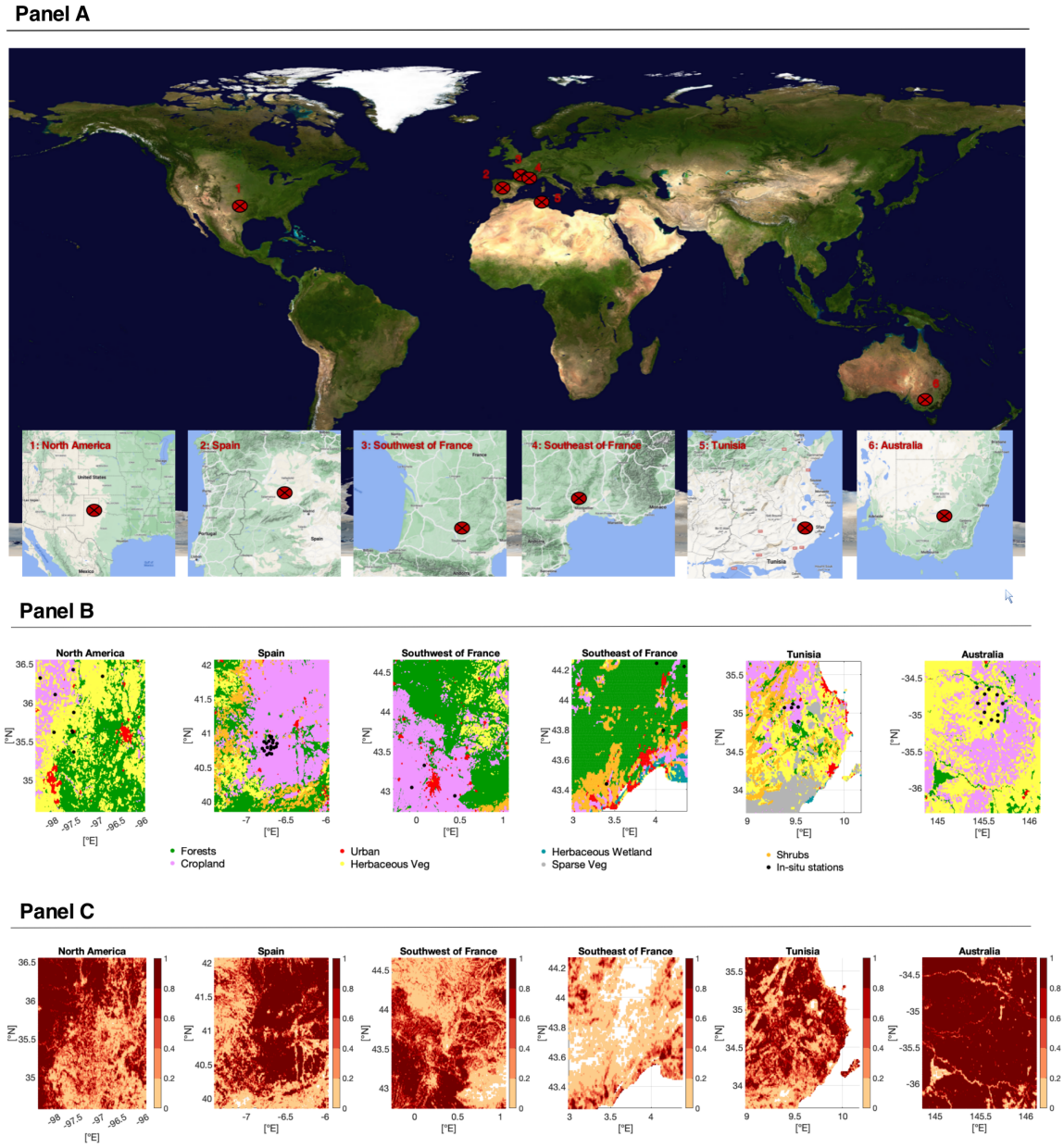

Figure 1. **Panel A:** Global locations of the 6 regions of study. **Panel B:** Copernicus land cover maps of the 6 regions of study aggregated at 1-km spatial resolution. Only the dominant land cover type within a 1-km^2 pixel is shown. For instance, a pixel characterised as forests can contain 27% of forests, 26% of croplands, 24% of herbaceous vegetation and 23% of shrublands, or 90% of forests and 10% of herbaceous vegetation. The in-situ stations are shown as black dots. One black dot can correspond to several sensors since some of them have the same coordinates. **Panel C:** Proportion of croplands and herbaceous vegetation within each 1-km^2 pixel for the 6 regions of study. The proportion is expressed as a percentage ranging from 0 to 1. Pixels with no cropland or herbaceous vegetation at all are shown as white areas.

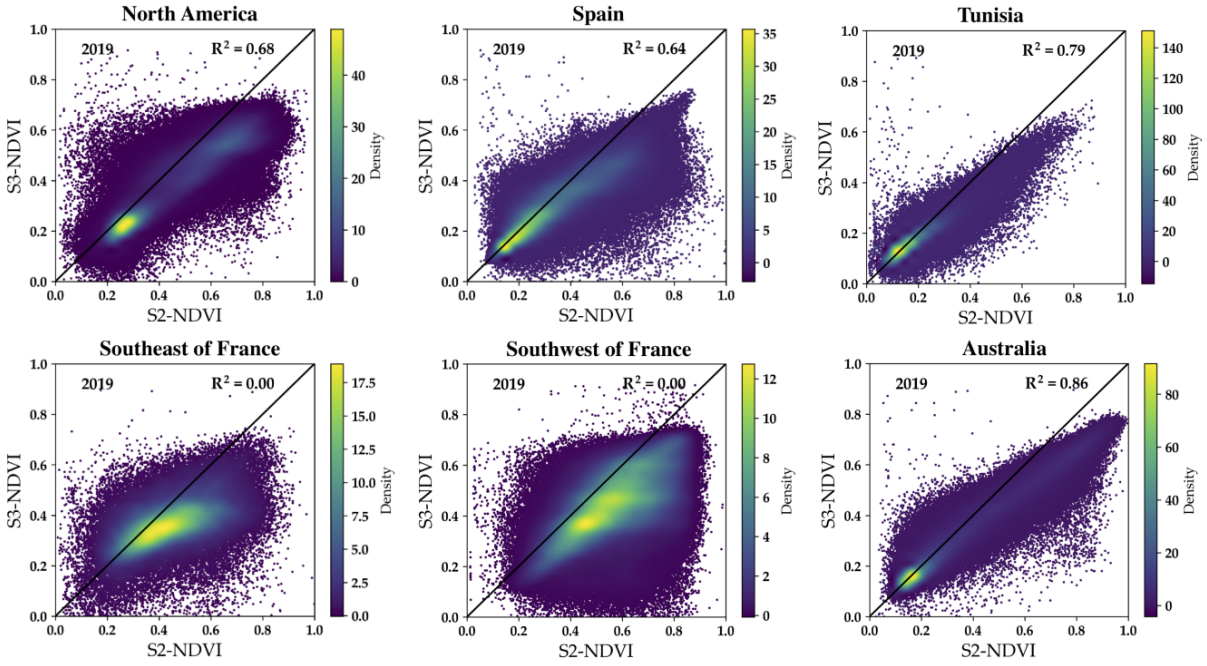

Figure 2. Correlation between S2 and S3 NDVI at 1-km grid scale ~~over one year~~ for the 6 study ~~sites.~~regions from January to December 2019.

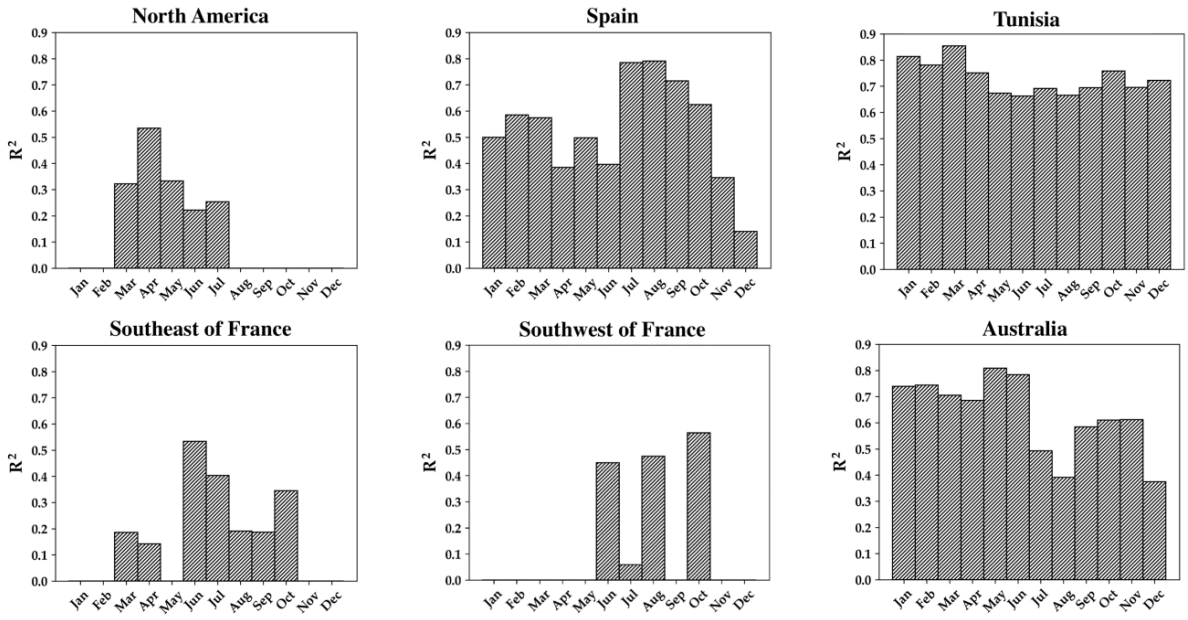

Figure 3. Correlation between S2 and S3 NDVI at 1-km grid scale each month for the 6 study ~~sites.~~ regions from January to December 2019. Months having no bars means that there is no correlation between S2 and S3 NDVI.

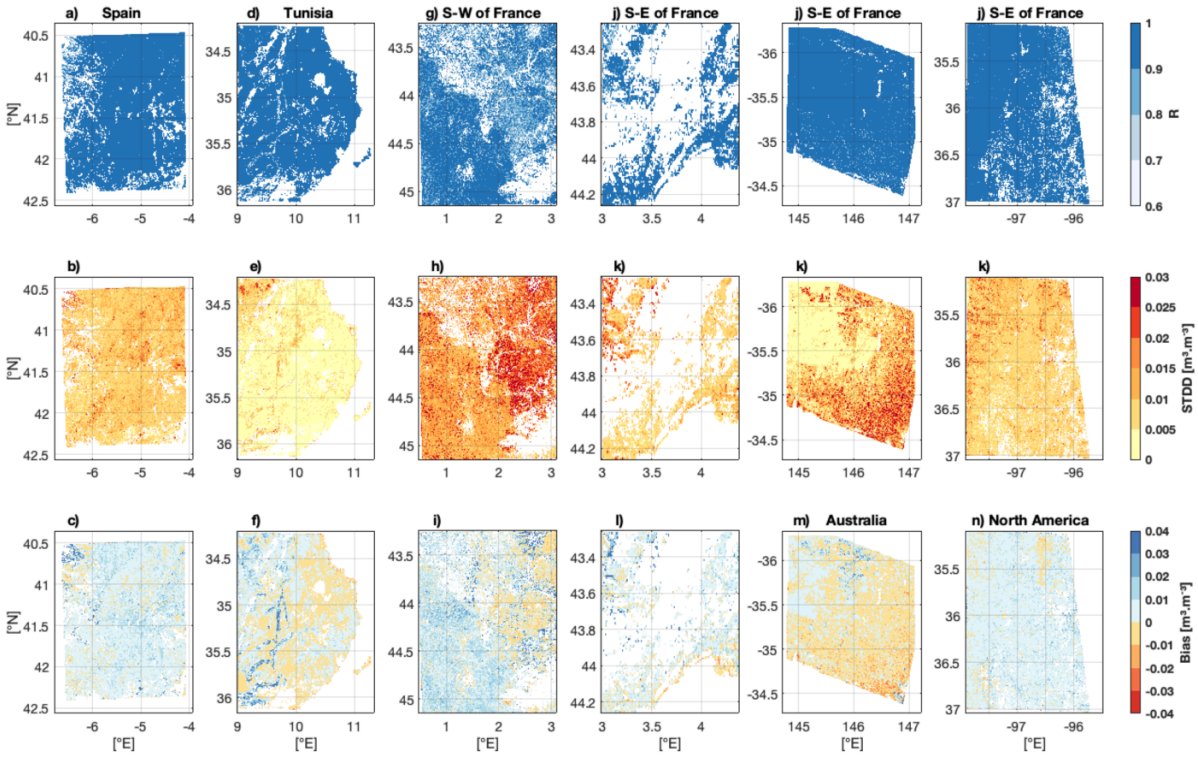

Figure 4. Comparison of S^2MP_{S1S3} with respect to S^2MP_{S1S2} over the regions of study in terms of Pearson correlation (R) as well as bias (S^2MP_{S1S2} minus S^2MP_{S1S3}) and standard deviation of the difference ($STDD$) in $m^3\ m^{-3}$. The analysis was performed from January to December 2019.

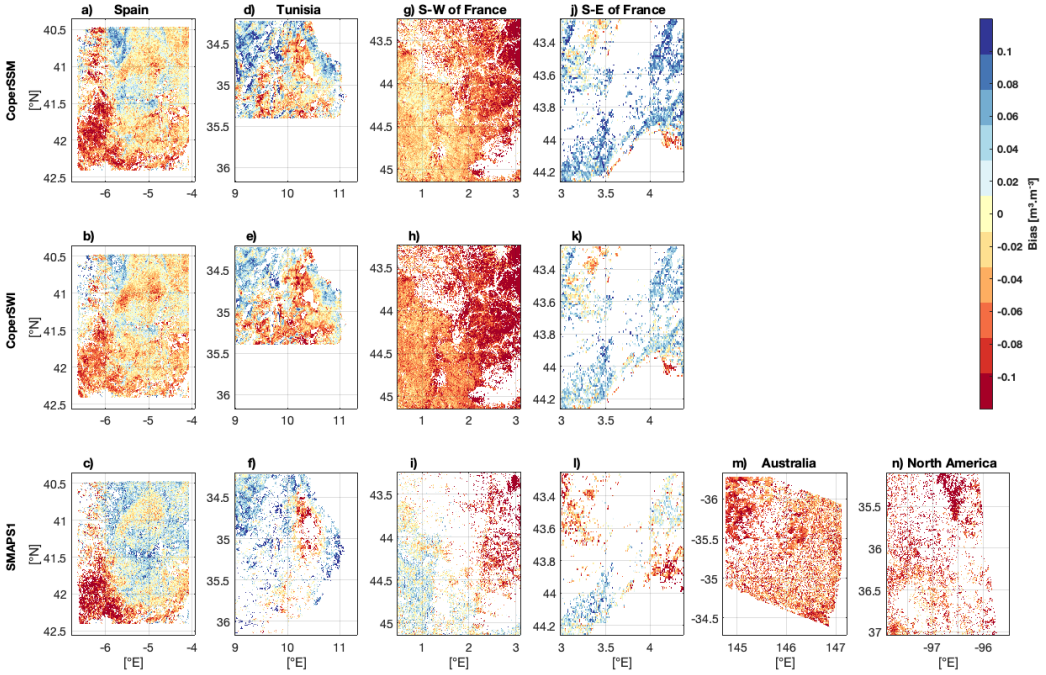

Figure 5. Comparison of ~~S^2MP_{S1S2}~~ S^2MP_{S1S3} with respect to $CoperSSM$ (~~S^2MP_{S1S2}~~ S^2MP_{S1S3} minus $CoperSSM$), $CoperSWI$ (~~S^2MP_{S1S2}~~ S^2MP_{S1S3} minus $CoperSWI$) and $SMAPS1$ (~~S^2MP_{S1S2}~~ S^2MP_{S1S3} minus $SMAPS1$) over the regions of study in terms of bias in $m^3\ m^{-3}$. The analysis was performed from January to December 2019.

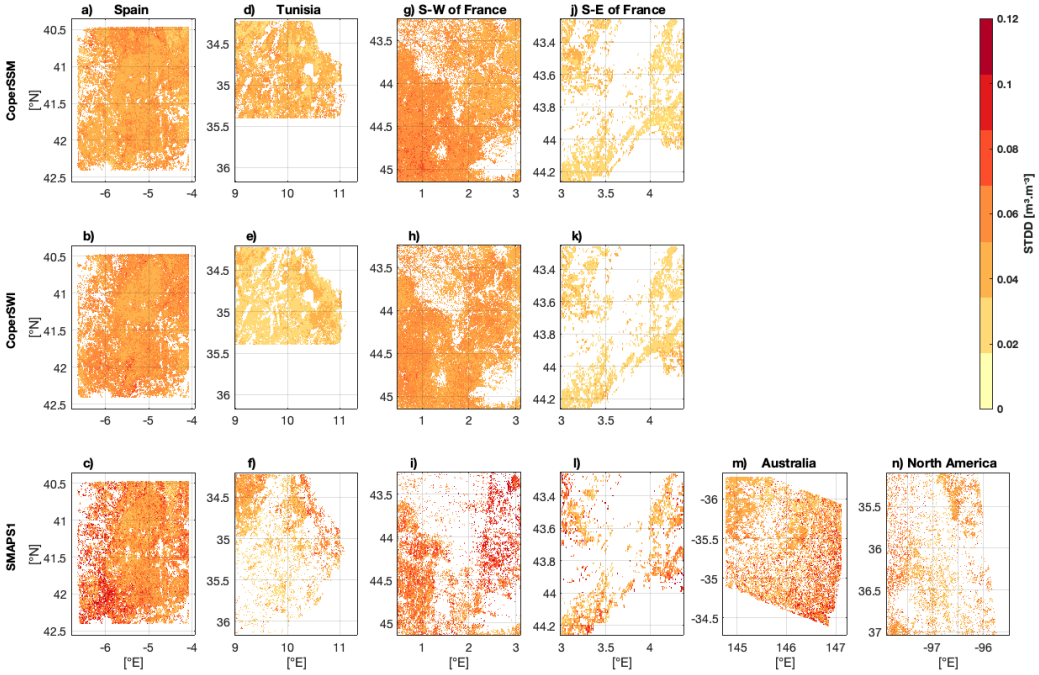

Figure 6. Comparison of ~~S^2MP_{S1S2}~~ S^2MP_{S1S3} with respect to $CoperSSM$, $CoperSWI$ and $SMAPS1$ over the regions of study in terms of standard deviation of the difference ($STDD$) in $m^3\ m^{-3}$. The analysis was performed from January to December 2019.

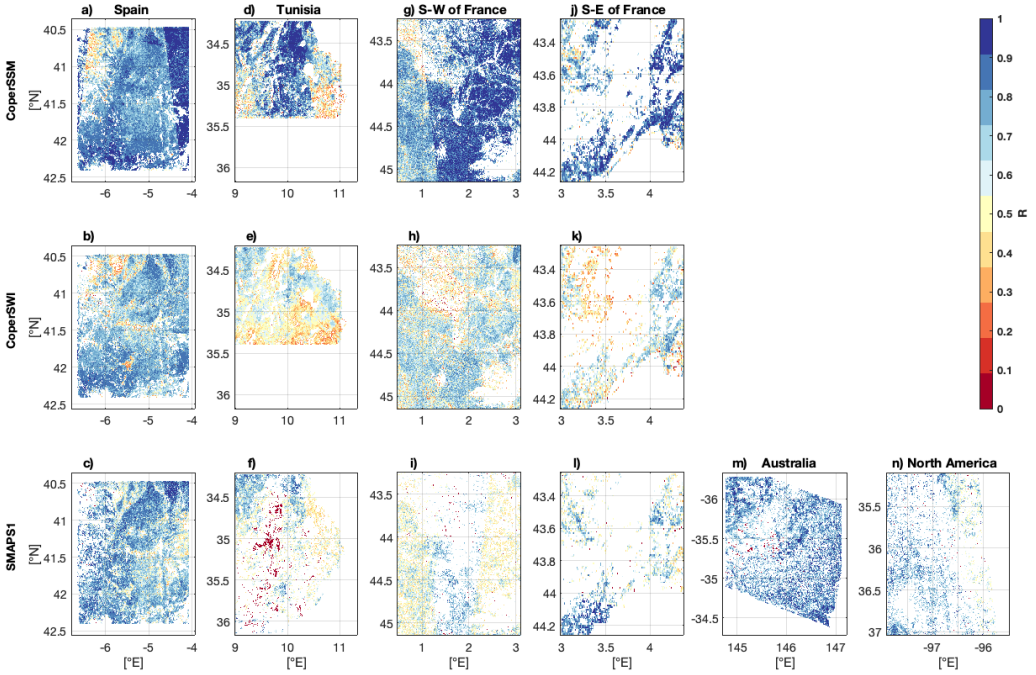

Figure 7. Comparison of ~~S^2MP_{S1S2}~~ S^2MP_{S1S3} with respect to $CoperSSM$, $CoperSWI$ and $SMAPS1$ over the regions of study in terms of Pearson correlation (R). The analysis was performed from January to December 2019.

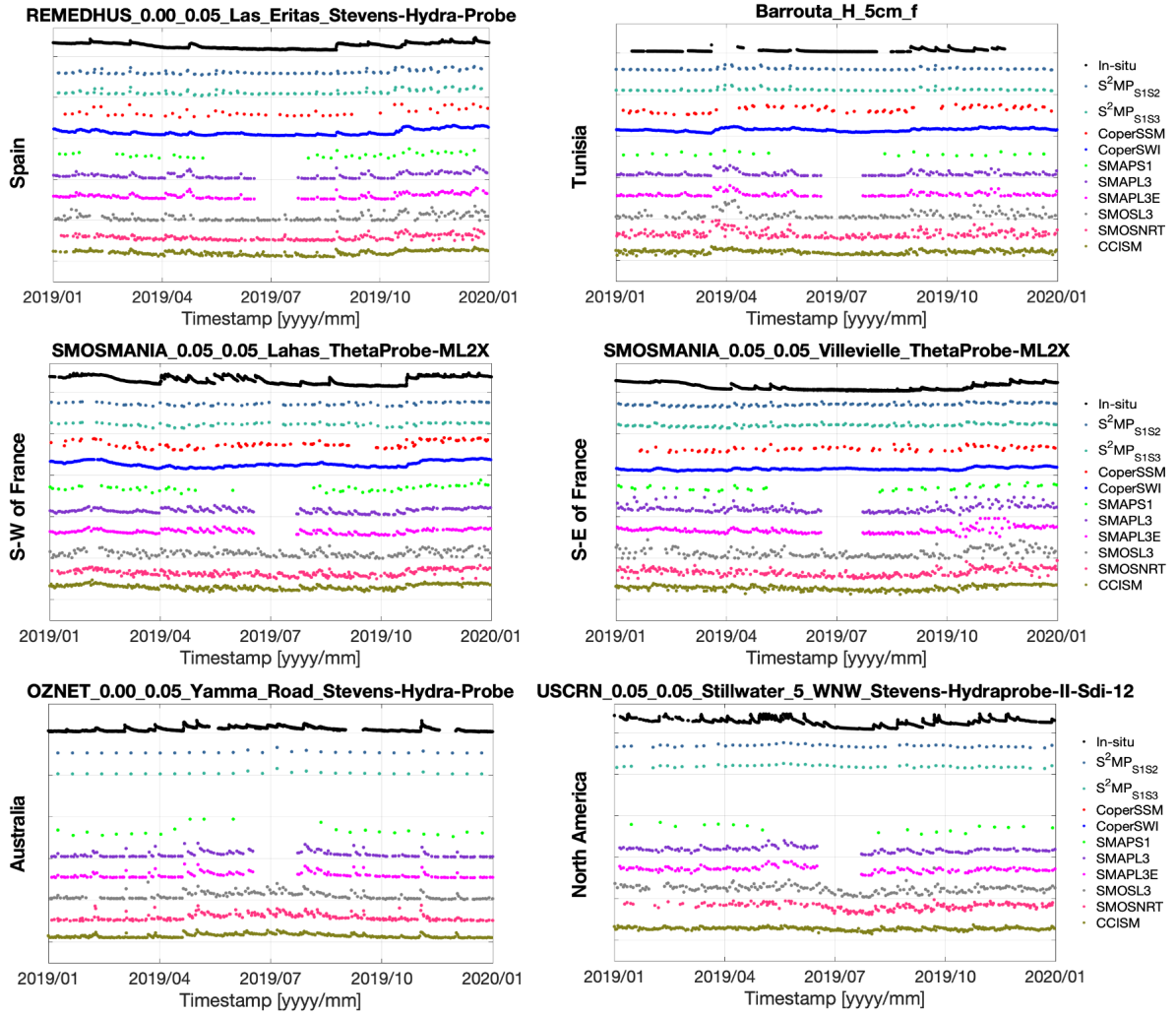

Figure 8. Examples of SM time series from the different HR and CR datasets at 6 in-situ stations (one for each region).

Table 2. Comparison of ~~S^2MP_{S1S2}~~ S^2MP_{S1S3} against ~~the HR SM products~~ $CoperSSM$, $CoperSWI$ and $SMAPS1$, in terms of ~~Pearson correlation (R)~~, bias and $STDD$, over 1-km^2 pixels where croplands ~~and~~ or herbaceous vegetation are the dominant land cover classes, respectively. ~~M stands for "mixed" pixels in which croplands or herbaceous vegetation~~ The metrics are also derived according to the ~~dominant~~ degree of coverage of the land cover~~classes in any proportion while H stands for "homogeneous"~~. One set of metrics is computed considering only pixels ~~, in which at least~~ covered by less than 75% of ~~the 1-km^2 area~~ croplands or herbaceous vegetation. Another set of metrics is computed considering only pixels covered by at least 75% of croplands or herbaceous vegetation. ~~Only median values are shown.~~ The analysis was performed from January to December 2019.

Regions	**Products**	**Croplands**						**Herbaceous vegetation**					
		$<$ 75%			**$\geq$ 75%**			**$<$ 75%**			**$\geq$ 75%**		
		R	$Bias$	$STDD$	R	$Bias$	$STDD$	R	$Bias$	$STDD$	R	$Bias$	$STDD$
Spain	$CoperSSM$	0.63	0.01	0.06	0.72	0.01	0.06	0.67	0.06	0.06	0.69	0.07	0.06
	$CoperSWI$	0.61	0.01	0.06	0.68	0.01	0.06	0.65	0.04	0.06	0.70	0.06	0.06
	$SMAPS1$	0.54	-0.01	0.07	0.65	-0.01	0.06	0.64	0.06	0.08	0.71	0.09	0.08
Tunisia	$CoperSSM$	0.37	-0.02	0.06	0.55	-0.01	0.05	0.32	-0.01	0.06	0.31	-0.01	0.06
	$CoperSWI$	0.37	0	0.05	0.45	-0.01	0.05	0.36	0.01	0.05	0.34	0.01	0.05
	$SMAPS1$	0.38	-0.03	0.07	0.51	-0.03	0.06	0.32	-0.02	0.07	0.27	-0.01	0.07
Southwest of France	$CoperSSM$	0.56	0.03	0.06	0.71	0.03	0.06	0.69	0.07	0.06	0.62	0.09	0.06
	$CoperSWI$	0.48	0.06	0.06	0.59	0.05	0.06	0.55	0.09	0.06	0.58	0.09	0.06
	$SMAPS1$	0.28	0.01	0.09	0.48	-0.01	0.07	0.36	0.09	0.10	0.34	0.11	0.10
Southeast of France	$CoperSSM$	0.63	-0.04	0.04	0.75	-0.05	0.03	0.44	0.02	0.05	0.72	0.06	0.02
	$CoperSWI$	0.47	-0.03	0.04	0.56	-0.03	0.04	0.48	0.06	0.05	-	-	-
	$SMAPS1$	0.45	0.02	0.07	0.45	0.04	0.08	0.49	0.04	0.05	-	-	-
Australia	$CoperSSM$	-	-	-	-	-	-	-	-	-	-	-	-
	$CoperSWI$	-	-	-	-	-	-	-	-	-	-	-	-
	$SMAPS1$	0.56	0.05	0.06	0.59	0.05	0.06	0.55	0.05	0.06	0.60	0.06	0.05
North America	$CoperSSM$	-	-	-	-	-	-	-	-	-	-	-	-
	$CoperSWI$	-	-	-	-	-	-	-	-	-	-	-	-
	$SMAPS1$	0.68	0.07	0.06	0.71	0.08	0.06	0.58	0.06	0.06	0.53	0.09	0.06

Table 3. Evaluation of the HR and CR SM time series against in-situ measurements in ~~situ data in~~ terms of Pearson correlation (R,R^a), bias (remotely sensed minus ground based SM in [m^3 $m^{~~-3~~-3}$]) and standard deviation of the difference ($STDD$ in [m^3 m^{-3}]). The metrics were computed by taking into account the 6 regions of study together and only the median values are shown here. The symbol * indicates the HR ~~data sets~~ datasets averaged at 25-km resolution.The analysis was performed from January to December 2019.

Products	R	R^a	$Bias$	$STDD$
Sentinel-only high resolution data				
S^2MP_{S1S2}	~~0.48~~ 0.59	0.36	~~0.003~~ -0.06	0.05
S^2MP_{S1S3}	0.56	0.37	-0.06	0.06
$CoperSSM$	~~0.44~~ 0.53	~~0.25~~ 0.18	~~0.05~~ 0.04	0.08
Merged high resolution data				
$CoperSWI$	~~0.64~~ 0.74	~~0.49~~ 0.46	~~0.06~~ 0.05	0.05
$SMAPS1$	~~0.60~~ 0.64	~~0.26~~ 0.35	~~-0.001~~ -0.03	~~0.07~~ 0.06
Coarse resolution data				
$SMAPL3$	~~0.68~~ 0.81	~~0.43~~ 0.55	~~0.005~~ -0.05	0.05
$SMAPL3E$	~~0.68~~ 0.81	~~0.46~~ 0.52	~~0.002~~ -0.05	0.05
$SMOSL3$	~~0.65~~ 0.69	~~0.30~~ 0.49	~~0.01~~ -0.03	~~0.07~~ 0.06
$SMOSNRT$	~~0.67~~ 0.76	~~0.33~~ 0.45	~~-0.004~~ -0.02	~~0.06~~ 0.05
$CCISM$	~~0.68~~ 0.73	~~0.40~~ 0.48	~~0.07~~ 0.03	~~0.04~~ 0.05
High resolution data aggregated to coarse resolution				
$S^2MP^*_{S1S2}$	~~0.49~~ 0.58	~~0.33~~ 0.38	~~0.01~~ -0.06	~~0.05~~ 0.06
$S^2MP^*_{S1S3}$	0.56	0.38	-0.05	0.06
$CoperSSM^*$	~~0.43~~ 0.53	~~0.22~~ 0.20	0.05	0.07
$CoperSWI^*$	~~0.63~~ 0.73	~~0.48~~ 0.47	~~0.06~~ 0.05	0.05
$SMAPS1^*$	~~0.69~~ 0.79	~~0.32~~ 0.44	~~0.01~~ -0.02	~~0.05~~ 0.04

References

Al Bitar, A., Mialon, A., Kerr, Y., Cabot, F., Richaume, P., Jacquette, E., Quesney, A., Mahmoodi, A., Tarot, S., Parrens, M., Al-yaari, A., Pellarin, T., Rodriguez-Fernandez, N., and Wigneron, J.-P.: The Global SMOS Level 3 daily soil moisture and brightness temperature maps, Earth System Science Data, 9, 293–315, https://doi.org/10.5194/essd-2017-1, 2017.

Albergel, C., Rüdiger, C., Pellarin, T., Calvet, J. C., Fritz, N., Froissard, F., and Martin, E.: From near-surface to root-zone soil moisture using an exponential filter: an assessment of the method based on in-situ observations and model simulations., Hydrology and Earth System Sciences, 12(6), 1323–1337, 2008.

Baghdadi, N., Holah, N., and Zribi, M.: Calibration of the integral equation model for SAR data in C-band and HH and VV polarizations., Remote Sensing, 27, 805–816, 2006.

Baghdadi, N., Chaaya, J., and Zribi, M.: Semiempirical calibration of the integral equation model for SAR data in C-band and cross polarization using radar images and field measurements., IEEE Geosci. Remote Sens. Lett., 8, 14–18, 2011.

Baghdadi, N., El Hajj, M., and Zribi, M.and Bousbih, S.: Calibration of the Water Cloud Model at C-Band for Winter Crop Fields and Grasslands., Remote Sensing, 9, 969, 2017.

Balenzano, A., Mattia, F., Satalino, G., and Davidson, M.: Dense Temporal Series of C- and L-band SAR Data for Soil Moisture Retrieval Over Agricultural Crops., IEEE J. Sel. Top. Appl. Earth Obs. Remote Sens., 4, 439–450, 2010.

Bauer-Marschallinger, B., Paulik, C., Hochstöger, S., Mistelbauer, T., Modanesi, S., Ciabatta, L., Massari, C., Brocca, L., and Wagner, W.: Soil Moisture from Fusion of Scatterometer and SAR: Closing the Scale Gap with Temporal Filtering., Remote Sensing, pp. 1 – 20, https://doi.org/DOI 10.3390/rs10071030, 2018.

Bauer-Marschallinger, B., Freeman, V., Cao, S., Paulik, C., Schaufler, S., Stachl, T., Modanesi, S., Massari, C., Ciabatta, L., Brocca, L., and Wagner, W.: Toward Global Soil Moisture Monitoring With Sentinel-1: Harnessing Assets and Overcoming Obstacles., IEEE Transactions on Geoscience and Remote Sensing, pp. 1 – 20, https://doi.org/DOI 10.1109/TGRS.2018.2858004, 2019.

Bazzi, H., Baghdadi, N., El Hajj, M., Zribi, M., and Belhouchette, H.: A Comparison of Two Soil Moisture Products S2MP and Copernicus-SSM over Southern France., Journal of Selected Topics in Applied Earth Observations and Remote Sensing, https://doi.org/doi: 10.1109/JSTARS.2019.2927430, 2019.

Bell, J., Palecki, M., Baker, C., Collins, W., Lawrimore, J., Leeper, R., Hall, M., Kochendorfer, J., Meyers, T., Wilson, T., and Diamond, H.: U.S. Climate Reference Network soil moisture and temperature observations., J. Hydrometeorol., 14, 977–988, 2013.

Bousbih, S., Zribi, M., Lili-Chabaane, Z., Baghdadi, N., El Hajj, M., Gao, Q., and Mougenot, B.: Potential of Sentinel-1 Radar Data for the Assessment of Soil and Cereal Cover Parameters., Sensors, 17, 2617, 2017.

Brocca, L., Hasenauer, S., Lacava, T., Melone, F., Moramarco, T., Wagner, W., Dorigo, W., Matgen, P., Martínez-Fernández, J., Llorens, P., Latron, J., Martin, C., and M, B.: Soil moisture estimation through ASCAT and AMSR-E sensors: An intercomparison and validation study across Europe, Remote Sensing of Environment, 115, 3390–3408, 2011.

Buchhorn, M., Bertels, L., Smets, B., De Roo, B., Lesiv, M., Tsendbazar, N. E., Masiliunas, D., and Li, L.: Copernicus Global Land Service: Land Cover 100m: version 3 Globe 2015-2019: Algorithm Theoretical Basis Document, https://doi.org/DOI 10.5281/zenodo.3606361, 2020.

Calvet, J.-C., Fritz, N., Froissard, F., Suquia, D., Petitpa, A., and Piguet, B.: In situ soil moisture observations for the CAL/VAL of SMOS: The SMOSMANIA network, in: Geoscience and Remote Sensing Symposium, 2007. IGARSS 2007. IEEE International, pp. 1196–1199, IEEE, 2007.

Chan, S., Njoku, E. G., and Colliander, A.: SMAP L1C Radiometer Half-Orbit 36 km EASE-Grid Brightness Temperatures, Version 4., Boulder, Colorado USA. NASA National Snow and Ice Data Center, https://doi.org/https://doi.org/10.5067/ZVILG0PS6CTI., 2018.

Cook, D.: Surface Energy Balance System (SEBS) Instrument Handbook, Tech. rep., DOE Office of Science Atmospheric Radiation Measurement (ARM) Program, 2018.

Cook, D. R.: Soil Water and Temperature System (SWATS) Instrument Handbook, Tech. rep., DOE Office of Science Atmospheric Radiation Measurement (ARM) Program, 2016.

Das, N., Entekhabi, D., Dunbar, S., Chaubell, J., Colliander, A., Yueh, S., Jagdhuber, T., Chen, F., Crow, W. T., O'Neill, P. E., Walker, J., Berg, A., Bosch, D., Caldwell, T., Cosh, M., Collins, C. H., Lopez-Baeza, E., and Thibeault., M.: The SMAP and Copernicus Sentinel 1A/B microwave active-passive high resolution surface soil moisture product, Remote Sensing of Environment. 233. 111380., https://doi.org/doi: https://doi.org/10.1016/j.rse., 2019.

Das, N., Entekhabi, D., Dunbar, R. S., Kim, S., Yueh, S., Colliander, A., O'Neill, P. E., Jackson, T., Jagdhuber, T., Chen, F., Crow, W. T., Walker, J., Berg, A., Bosch, D., Caldwell, T., , and Cosh, M.: SMAP/Sentinel-1 L2 Radiometer/Radar 30-Second Scene 3 km EASE-Grid Soil Moisture, Version 3, Boulder, Colorado USA. NASA National Snow and Ice Data Center Distributed Active Archive Center., https://doi.org/doi: https://doi.org/10.5067/ASB0EQO2LYJV., 2020.

De Rosnay, P., Drusch, M., Vasiljevic, D., Balsamo, G., Albergel, C., and Isaksen, L.: A simplified Extended Kalman Filter for the global operational soil moisture analysis at ECMWF, Quarterly Journal of the Royal Meteorological Society, 139, 1199–1213, 2013.

de Rosnay, P., Balsamo, G., Albergel, C., Muñoz-Sabater, J., and Isaksen, L.: Initialisation of land surface variables for numerical weather prediction, Surveys in Geophysics, 35, 607–621, 2014.

Donlon, C., Berruti, B., Mecklenberg, S., Nieke, J., Rebhan, H., Klein, U., Buongiorno, A., Mavrocordatos, C., Frerick, J., Seitz, B., Goryl, P., Féménias, P., Stroede, J., and Sciarra, R.: The Sentinel-3 Mission: Overview and status, in: 2012 IEEE International Geoscience and Remote Sensing Symposium, pp. 1711–1714, https://doi.org/10.1109/IGARSS.2012.6351194, 2012.

Dorigo, W., Wagner, W., Hohensinn, R., Hahn, S., Paulik, C., Xaver, A., Gruber, A., Drusch, M., Mecklenburg, S., Oevelen, P. v., et al.: The International Soil Moisture Network: a data hosting facility for global in situ soil moisture measurements, Hydrology and Earth System Sciences, 15, 1675–1698, 2011.

Dorigo, W., Wagner, W., Albergel, C., Albrecht, F., Balsamo, G., Brocca, L., Chung, D., Ertl, M., Forkel, M., Gruber, A., et al.: ESA CCI Soil Moisture for improved Earth system understanding: State-of-the art and future directions, Remote Sensing of Environment, 203, 185–215, 2017.

Dorigo, W., Himmelbauer, I., and Aberer, D.: The International Soil Moisture Network: serving Earth system science for over a decade, Hydrology and Earth System Sciences, https://doi.org/https://doi.org/10.5194/hess-2021-2, 2021.

El Hajj, M., Baghdadi, N., Zribi, M., and Bazzi, H.: Synergic use of Sentinel-1 and Sentinel-2 images for operational soil moisture mapping at high spatial resolution over agricultural areas., Remote Sensing, 9, 1292, https://doi.org/doi:10.3390/rs9121292, 2017.

El Hajj, M., Baghdadi, N., Zribi, M., Rodríguez-Fernández, N., Wigneron, J. P., Al-Yaari, A., Al Bitar, A., Albergel, C., and Calvet, J. C.: Evaluation of SMOS, SMAP, ASCAT and Sentinel-1 Soil Moisture Products at Sites in Southwestern France., Remote Sensing, 10(4), 569, 2018.

Entekhabi, D., Njoku, E. G., O'Neill, P. E., Kellogg, K. H., Crow, W. T., Edelstein, W. N., Entin, J. K., Goodman, S. D., Jackson, T. J., Johnson, J., et al.: The soil moisture active passive (SMAP) mission, Proceedings of the IEEE, 98, 704–716, 2010.

Entekhabi, D., Yueh, S., O'Neill, P. E., and Kellogg, K. H.: SMAP Handbook, Tech. rep., Jet Propulsion Laboratory, NASA, 2014.

GCOS: The Status of the Global Climate Observing System 2021, Tech. rep., Global Climate Observing System, World Meteorological Organization, Report 240, 2021.

Gonzalez-Zamora, A., Sanchez, N., Pablos, M., and Martinez-Fernandez, J.: CCI soil moisture assessment with SMOS soil moisture and in situ data under different environmental conditions and spatial scales in Spain., Remote Sensing of Environment, 255, 2018.

Gorrab, A., Zribi, M., Baghdadi, N., Mougenot, B., and Lili-Chaabane, Z.: Retrieval of both soil moisture and texture using TerraSAR-X images., Remote Sensing, 7, 10 098–10 116, https://doi.org/doi:10.3390/rs70810098, 2015.

Gruber, A., Scanlon, T., van der Schalie, R., Wagner, W., and Dorigo, W.: Evolution of the ESA CCI Soil Moisture climate data records and their underlying merging methodology, Earth System Science Data, pp. 1–37, 2019.

Guerif and Duke: Adjustment procedures of a crop model to the site specific characteristics of soil and crop using remote sensing data assimilation, Agriculture Ecosystems & Environment, pp. 57–69, 2000.

Hajj, M., Baghdadi, N., Belaud, G., Zribi, M., Cheviron, B., Courault, D., Hagolle, O., and Charron, F.: Irrigated Grassland Monitoring Using a Time Series of TerraSAR-X and COSMO-SkyMed X-Band SAR Data., Remote Sens., 6, 10 002–10 032, 2014.

Henocq, C., North, P., Heckel, A., Ferron, S., Lamquin, N., Dransfeld, S., Bourg, L., TOTE, C., and Ramon, D.: OLCI/SLSTR SYN L2 Algorithm and Products Overview, in: IGARSS 2018 - 2018 IEEE International Geoscience and Remote Sensing Symposium, pp. 8723–8726, https://doi.org/10.1109/IGARSS.2018.8517420, 2018.

Imaoka, K., Kachi, M., Kasahara, M., Ito, N., Nakagawa, K., and Oki, T.: Instrument performance and calibration of AMSR-E and AMSR2, Remote Sensing and Spatial Information Sciences, 38., 2000.

Kerr, Y., Waldteufel, P., Wigneron, J.-P., Delwart, S., Cabot, F., Boutin, J., Escorihuela, M.-J., Font, J., Reul, N., Gruhier, C., Juglea, S., Drinkwater, M., Hahne, A., Martin-Neira, M., and Mecklenburg, S.: The SMOS Mission: New Tool for Monitoring Key Elements ofthe Global Water Cycle, Proceedings of the IEEE, 98, 666–687, https://doi.org/10.1109/JPROC.2010.2043032, 2010.

Kerr, Y., Waldteufel, P., Richaume, P., Wigneron, J., Ferrazzoli, P., Mahmoodi, A., Al Bitar, A., Cabot, F., Gruhier, C., Juglea, S., Leroux, D., Mialon, A., and Delwart, S.: The SMOS Soil Moisture Retrieval Algorithm, IEEE Transactions on Geoscience and Remote Sensing, 50, 1384–1403, https://doi.org/10.1109/TGRS.2012.2184548, 2012.

Kerr, Y. H., Waldteufel, P., Wigneron, J. P., Martinuzzi, J., Font, J., and Berger, M.: Soil moisture retrieval from space: the Soil Moisture and Ocean Salinity (SMOS) mission, IEEE Transactions on Geoscience and Remote Sensing, 39, 1729–1735, https://doi.org/10.1109/36.942551, 2001.

Kim, S., Liu, Y. Y., Johnson, F. M., Parinussa, R. M., and Sharma, A.: A global comparison of alternate AMSR2 soil moisture products: Why do they differ, Remote Sensing of Environment, 161, 43–62, 2015.

Koster, R. D., Dirmeyer, P. A., Guo, Z., Bonan, G., Chan, E., Cox, P., Gordon, C. T., Kanae, S., Kowalczyk, E., Lawrence, D., Liu, P., Lu, C.-H., Malyshev, S., McAvaney, B., Mitchell, K., Mocko, D., Oki, T., Oleson, K., Pitman, A., Sud, Y. C., Taylor, C. M., Verseghy, D., Vasic, R., Xue, Y., and Yamada, T.: Regions of strong coupling between soil moisture and precipitation, Science, 305, 1138–1140, 2004.

Leroux, D. J., Kerr, Y. H., Al Bitar, A., Bindlish, R., Jackson, T. J., Berthelot, B., and Portet, G.: Comparison between SMOS, VUA, ASCAT, and ECMWF soil moisture products over four watersheds in US, Geoscience and Remote Sensing, IEEE Transactions on, 52, 1562–1571, 2014.

Massari, C., Modanesi, S., Dari, J., Gruber, A., De Lannoy, G., Girotto, M., Quintana-Seguí, P., Le Page, M., Jarlan, L., Zribi, M., and Ouaadi, N.: A review of irrigation information retrievals from space and their utility for users, Remote Sensing, 13(20), 4112, 2021.

Merlin, O., Jacob, F., Wigneron, J. P., Walker, J., and Chehbouni, G.: Multidimensional Disaggregation of Land Surface Temperature Using High-Resolution Red, Near-Infrared, Shortwave-Infrared, and Microwave-L Bands, Geoscience and Remote Sensing, IEEE Transactions on, 50, 1864–1880, https://doi.org/10.1109/TGRS.2011.2169802, 2012.

Moran, M., Hymer, D., Qi, J., and E Sano, E.: Soil moisture evaluation using multi-temporal synthetic aperture radar (SAR) in semiarid rangeland., Agric. For. Meteorol., 105, 69–80, 2000.

Muñoz-Sabater, J., Dutra, E., Agustí-Panareda, A., Albergel, C., Arduini, G., Balsamo, G., Boussetta, S., Choulga, M., Harrigan, S., Hersbach, H., et al.: ERA5-Land: A state-of-the-art global reanalysis dataset for land applications, Earth System Science Data, 13, 4349–4383, 2021.

Notarnicola, C., Angiulli, M., and Posa, F.: Soil Moisture Retrieval From Remotely Sensed Data: Neural Network Approach Versus Bayesian Method, Geoscience and Remote Sensing, IEEE Transactions on, 46, 547–557, https://doi.org/10.1109/TGRS.2007.909951, 2008.

Ojha, N., Merlin, O., Suere, C., and Escorihuela, M. J.: Extending the spatio-temporal applicability of DISPATCH soil moisture downscaling algorithm: A study case using SMAP, MODIS and Sentinel-3 data, Frontiers in Environmental Science, 9, 2021.

O'Neill, P. E., Chan, S., Njoku, E. G., Jackson, T., and Bindlish, R.: SMAP L2 Radiometer Half-Orbit 36 km EASE-Grid Soil Moisture, Version 5., NASA National Snow and Ice Data Center Distributed Active Archive Center, 2018.

O'Neill, P. E., Chan, S., Njoku, E. G., Jackson, T., Bindlish, R., and Chaubell, J.: SMAP Enhanced L3 Radiometer Global Daily 9 km EASE-Grid Soil Moisture, Version 1., Boulder, Colorado USA. NASA National Snow and Ice Data Center Distributed Active Archive Center., 2019a.

O'Neill, P. E., Chan, S., Njoku, E. G., Jackson, T., Bindlish, R., and Chaubell, J.: SMAP L3 Radiometer Global Daily 36 km EASE-Grid Soil Moisture, Version 6., NASA National Snow and Ice Data Center Distributed Active Archive Center, 2019b.

Paloscia, S., Santi, E., Pettinato, S., and Angiulli, M.: Soil properties estimates from SAR data by using a bayesian approach combined with IEM, Proceedings of the IEEE International Conference on Automation and Logistics Qingdao, China September 2008, 2, 819–822, https://doi.org/10.1109/IGARSS.2004.1368530, 2004.

Paulik, C., Dorigo, W., Wagner, W., and Kidd, R.: Validation of the ASCAT Soil Water Index using in situ data from the International Soil Moisture Network., International journal of applied earth observation and geoinformation, 30, 1–8, 2014.

Peng, J., Albergel, C., Balenzano, A., Brocca, L., Cartus, O., Cosh, M. H., and Loew, A.: A roadmap for high-resolution satellite soil moisture applications–confronting product characteristics with user requirements., Remote Sensing of Environment, 252, 112 162, 2020.

Pierdicca, N., Pulvirenti, L., and Bignami, C.: Soil moisture estimation over vegetated terrains using multitemporal remote sensing data., Remote Sens. Environ., 114, 440–448, 2010.

Plummer, S., Lecomte, P., and Doherty, M.: The ESA Climate Change Initiative (CCI): A European contribution to the generation of the Global Climate Observing System, Remote Sensing of Environment, 203, 2–8, 2017.

Rodell, M., Houser, P. R., U, J., Gottschalck, J., Mitchell, K., Meng, C.-J., Arsenault, K., Cosgrove, B., Radakovich, J., Bosilovich, M., Entin, J. K., Walker, J. P., Lohmann, D., and Tol, D.: The global land data assimilation system, American Meteorological Society, pp. 381–394, 2004.

Rodríguez-Fernández, N., de Rosnay, P., Albergel, C., Richaume, P., Aires, F., Prigent, C., and Kerr, Y.: SMOS neural network soil moisture data assimilation in a land surface model and atmospheric impact., Remote Sensing, 11(11), 1334, 2019.

Rodríguez-Fernández, N. J., Muñoz-Sabater, J., Richaume, P., Albergel, C., de Rosnay, P., Kerr, Y. H., Drusch, M., and Mecklenburg, S.: SMOS near real time soil moisture product: Processor overview and first validation results, Hydrology and Earth System Sciences, 21, 5201–5216,, 2017.

Smith, A. B., Walker, J. P., Western, A. W., Young, R. I., Ellett, K. M., Pipunic, R. C., Grayson, R. B., Siriwardena, L., Chiew, F. H. S., and H, R.: The Murrumbidgee soil moisture monitoring network data set, Water Resour. Res., 48, https://doi.org/10.1029/2012WR011976, 2012.

Spoto, F., Sy, O., Laberinti, P., Martimort, P., Fernandez, V., Colin, O., Hoersch, B., and Meygret, A.: Overview Of Sentinel-2, in: 2012 IEEE International Geoscience and Remote Sensing Symposium, pp. 1707–1710, https://doi.org/10.1109/IGARSS.2012.6351195, 2012.

Srivastava, H., Patel, P., Sharma, Y., and Navalgund, R.: Large-Area Soil Moisture Estimation Using Multi-Incidence-Angle RADARSAT-1 SAR Data., IEEE Trans. Geosci. Remote Sens., 47, 2528–2535, 2009.

Tomer, S. K., Al Bitar, A., Sekhar, M., Zribi, M., Bandyopadhyay, S., and Kerr, Y.: MAPSM: A spatio-temporal algorithm for merging soil moisture from active and passive microwave remote sensing, Remote Sensing, 8, 990, 2016.

Ulaby, F. T., Moore, R. K., and Fung, A. K.: Microwave Remote Sensing Active and Passive-Volume III: From Theory to Applications, Artech House, Inc, 1986.

Van der Schalie, R., Kerr, Y., Wigneron, J., Rodríguez-Fernández, N., Al-Yaari, A., and de Jeu, R.: Global SMOS soil moisture retrievals from the land parameter retrieval model, International Journal of Applied Earth Observation and Geoinformation, 45, 125–134, 2016.

Van der Schalie, R., de Jeu, R., Kerr, Y., Wigneron, J., Rodríguez-Fernández, N., Al-Yaari, A., Parinussa, R., Mecklenburg, S., and Drusch, M.: The merging of radiative transfer based surface soil moisture data from SMOS and AMSR-E, Remote Sensing of Environment, 189, 180–193, 2017.

Vreugdenhil, M., Dorigo, W. A., Wagner, W., De Jeu, R. A., Hahn, S., and Van Marle, M. J.: Analyzing the vegetation parameterization in the TU-Wien ASCAT soil moisture retrieval, IEEE Transactions on Geoscience and Remote Sensing, 54, 3513–3531, 2016.

Wagner, W.: Soil Moisture Retrieval From ERS Scatterometer Data, Ph.D. thesis, Vienna University of Technology, 1998.

Wagner, W., Lemoine, G., and Rott, H.: A Method for Estimating Soil Moisture from ERS Scatterometer and Soil Data, Remote sensing of environment, 70, 191–207, https://doi.org/10.1016/S0034-4257(99)00036-X, 1999.

Wagner, W., Hahn, S., Kidd, R., Melzer, T., Bartalis, Z., Hasenauer, S., Figa-Saldaña, J., de Rosnay, P., Jann, A., Schneider, S., et al.: The ASCAT soil moisture product: A review of its specifications, validation results, and emerging applications, Meteorologische Zeitschrift, 22, 5–33, 2013.

Young, R., Walker, J., Yeoh, N., Smith, A., Ellett, K., Merlin, O., and Western, A.: Soil moisture and meteorological observations from the murrumbidgee catchment., Department of Civil and Environmental Engineering, The University of Melbourne., 2008.

Şekertekin, A., Marangoz, A., and Abdikan, S.: Soil Moisture Mapping Using Sentinel-1A Synthetic Aperture Radar Data., Int. J. Environ. Geoinform., 5, 178–188, 2018.